Drainage reorganization induces deviations in the ~~width-area slope~~ scaling between ~~of~~ valley widths ~~and channels~~

Elhanan Harel[1], Liran Goren[1], Onn Crouvi[2], Hanan Ginat[3], and Eitan Shelef[4].

[1]Earth and Environmental Sciences, Ben-Gurion University of the Negev, Beer Sheva, 84105, Israel.
[2]Geological Survey of Israel, Yesha'yahu Leibowitz 32, Jerusalem 9692100, Israel.
[3]The Dead-Sea and Arava Science Center, Tamar regional council Dead-Sea mobile post 86910, Tamar regional council, Israel.
[4]Geology and Environmental Science, University of Pittsburgh, 4107 O'Hara Street, Pittsburgh, Pennsylvania 15260- 3332, United ~~states~~States.

Correspondence to: Harel E. (elhananh@post.bgu.ac.il)

Abstract. The width of valleys and channels affects the hydrology, ecology, and geomorphic functionality of drainage networks. In many studies, the width of valleys and/or channels (W) is estimated as ~~Valley and channel widths are often estimated through~~ a power-law function of the drainage area (A), $W = k_c A^d$ ~~scaling between width (W) and drainage area (A), and where lithologic variability or differential uplift rates dominate, width was suggested to scale with both slope (S) and drainage area, through the relation $W = k_b A^b S^\epsilon$~~. However, in fluvial systems that experience drainage reorganization, abrupt changes in drainage area distribution can result in valley or channel widths that are disproportional to their drainage areas. Such disproportionality may be more distinguished in valleys than in channels due to a longer adjustment timescale for valleys. Therefore, ~~Consequently, in such cases~~, the valley width-area ~~slope~~ scaling in reorganized drainages is expected to deviate ~~relative~~ from that of ~~to~~ drainages that did not experience reorganization.

To explore the effect of reorganization on valley width- drainage area ~~slope~~ scaling, we studied 12 valley sections in the Negev desert, Israel, categorized into undisturbed, beheaded, and reversed valleys. We found that the values of the drainage area exponents, ~~*b*~~*d*, are lower in the beheaded valleys relative to undisturbed valleys, but remain positive. Reversed valleys, in contrast, are characterized by negative *d* exponents, indicating valley narrowing with increasing drainage area. In the reversed category, we also explored the independent effect of channel slope (S) through the equation $= k_b A^b S^c$, which yielded negative and overall similar values for *b* and *c*.

~~differs between valley categories, and that reversed valleys are characterized by a negative *b* exponent, indicating valley narrowing with increasing drainage area.~~

A detailed study in one ~~of a~~ reversed valley section shows that the valley narrows downstream whereas the channel widens, suggesting that, as hypothesized, the channel width adjusts faster to post-reorganization drainage area distribution. The adjusted narrow channel dictates the width of formative flows in the reversed valley, which contrasts the meaningfully wider formative flows of the beheaded valley across the divide. ~~reveals that unlike the negative *b* exponent that links drainage area to valley width, the relation between drainage area and channel width is best fitted with a positive *b* exponent.~~ This difference results in ~~indicates that the timescale of channel width adjustment to post-~~

~~reorganization drainage area distribution is faster than that of the valley width adjustment. We find that the difference in channel width across the divide causes~~ a step change in the unit stream power between the ~~adjusted~~ reserved ~~channel~~ and ~~the unadjusted,~~ beheaded channels, potentially~~. Gradients in width and unit stream power across the divide,~~ leading to a "width-feedback" that promotes ongoing divide migration and reorganization.

Our findings demonstrate that valley width-area scaling is a potential tool for identifying~~The identified distinct width-area slope scaling of reorganized valleys could assist in recognizing and constraining the dynamics of~~ landscapes influenced by drainage reorganization. Accounting for reorganization-specific scaling can improve estimation ~~and likely has critical implications for the distribution~~ of erosion rates distributions in reorganized landscapes.

1 Introduction

The width of channels and their hosting valleys control river~~'s~~ dynamics and functionality with far-reaching implications across a wide range of disciplines, from flood ~~and seismic~~ hazards (e.g., Lóczy et al., 2009; Mashael Al, 2010; ~~Morell et al., 2020;~~ Sampson et al., 2015), to river ecosystems and habitats (e.g., Beeson et al., 2018; Brussock et al., 1985; May et al., 2013; Sweeney et al., 2004), and ~~to~~ hydrological modeling (e.g., Looper et al., 2012). Valley and channel width further play a central role in landscape evolution~~, as they respond to changes in the forcing that act on the landscape~~ (Amos and Burbank, 2007; Fisher et al., 2013; Hancock and Anderson, 2002). The ~~ratio~~ relation between valley width, which ~~integrates the~~ subsumes channels, terraces, and floodplains, ~~on the one hand, and morphometric valley properties such as~~other measures of the valley morphology including depth or fill thickness~~, on the other hand~~, are used to elucidate drainage evolution over geological timescales (e.g., Gibling, 2006; Schumm and Ethridge, 1994) and for inferring climate changes (Dury, 1964; Hancock and Anderson, 2002; Marcotte et al., 2021) and tectonic variations (Giaconia et al., 2012). The channel width is a key component in landscape evolution for its control on the shear stress exerted by the flowing water, sediment transport capacity, and erosion rate (Whittaker et al., 2007b; Yanites et al., 2010). Particularly, many landscape evolution and hydrologic models approximate the local erosion rate as a function of the channel stream power per unit channel width (i.e., unit stream power, Harbor, 1998; Lague, 2014; Magilligan et al., 2015; Turowski, 2018; Yanites, 2018).

The ~~wide use~~ central role of valley and channel width across ~~various~~ disciplines highlights the value of high-resolution width measurements, which could vary by several orders of magnitude within a single basin and across basins and landscapes (Schumm and Ethridge, 1994). ~~However, p~~Producing high-resolution field-based width measurement of channels and valleys is challenging and time-consuming~~.~~, and ~~In~~ in recent years, a growing body of work focused on developing tools for automatic width extraction based on remotely-sensed data (e.g., Fisher et al.,

2013; Gilbert et al., 2016; Hilley et al., 2020; Monegaglia et al., 2018; Roux et al., 2014; Rowland et al., 2016). Although these tools enabled a significant advancement in river research and management, they commonly focus on specific types of river morphology, and require parameter calibrations, as well as human supervision (Fryirs et al., 2019; Golly and Turowski, 2017). Due to these limitations, in many cases, width of natural channels and valleys is more commonly estimated based on the widely recognized scaling relationships between valley and channel widths and fundamental basin properties such as discharge (or its proxy, drainage area), which could be relatively easily measured from digital elevation models (e.g., Lavé and Avouac, 2001; Wobus et al., 2006). Furthermore, these channel width - drainage area scaling relationships are used frequently in landscape evolution models, where the channel width is parametrized based on the drainage area (e.g., Goren et al., 2014; Lague et al., 2014; Shobe et al., 2017; Yanites et al., 2013). However, studies that explored the channel width - drainage area scaling found that it is valid mostly under steady-state conditions, but is less reliable when lithologic, climatic and tectonic complexities are present in the landscape (Allen et al., 2013; Montgomery, 2004; Snyder and Kammer, 2008; Whipple et al., 2013; Yanites, 2018) Consequently, Beyond steady conditions, several studies demonstrated that width can adjust dynamically in response to transient environmental conditions (Snyder and Kammer, 2008; Whipple et al., 2013; Yanites, 2018), and that in such landscapes, a more complex scaling involving width, area, and slope might be more applicable. (Finnegan et al., 2005). The current study explores valley and channel width scaling in transient conditions that emerge from processes of drainage reorganization.

1.1 Width -area scaling relationsin channels and valleys

The common approach for channel width estimation relies on the seminal work of Leopold and Maddock (1953), who used empirical data to establish a power-law relation between the channel width, W [m] and discharge, Q [m^3/sec]. Based on the well-established correlation between discharge and drainage area, A [km], (e.g., Dunne and Leopold, 1978), the scaling between channel width and drainage area is often expressed as

$$W = k_c * A^d \quad (1)$$

Leopold and Maddock's relation, (Eq. (1)), was initially established for alluvial rivers, where d was found to be ~0.5. A similar scaling was later reported for bedrock rivers, with an exponent that typically ranges between 0.3–0.6 (Kirby and Ouimet, 2011; Montgomery and Gran, 2001; Snyder et al., 2003; Tomkin et al., 2003; Whitbread et

al., 2015; Yanites et al., 2010). The exponent's range was attributed to differences in rock properties, where more erodible and/or fractured ~~rocks~~ banks widen faster than resistant and/or intact ~~rocks~~ banks (Spotila et al., 2015; Whitbread et al., 2015; Wohl and Achyuthan, 2002; Wohl and David, 2008). Other studies invoked climatic variations and anthropogenic disturbances to explain variations in the *d* exponent (Bertrand and Liébault, 2019; Faustini et al., 2009; Snyder et al., 2003).

Although Eq. (1) is commonly used as an empirical relation, it is consistent with process-based theory. Channel widening is attributed to lateral bank erosion induced by particles impacting the channel wall (Li et al., 2020; Turowski, 2018) and is governed by the mechanical properties of the bedload and the channel banks, the channels' geometry, and the volume and trajectory of the bedload particles (e.g., Finnegan and Balco, 2013; Li et al., 2020; Yanites, 2018). Considering these controlling parameters, Turowski (2018) developed a model relating bedrock channel width to sediment supply, vertical erosion rate, and bank properties. Under spatially uniform erosion rate and steady-state conditions, Turowski's model predicts that the channel width is a power-law function of the drainage area, consistent with the form of Eq. (1).

Valley widening occurs when the channel migrates and abuts the valley wall, enabling particles from the channel to erode the valley wall. The effectiveness of valley widening is thus controlled by the frequency at which the channel abuts and erodes the valley wall, which depends on the valley width, channel width, and channel mobility within the valley (which increases with sediment flux) (Clubb et al., 2022). Despite the different processes that underlie the widening of channels and valleys, empirical observations~~Several studies~~ suggest~~ed~~ that the relation between the valley width and drainage area follows a similar power-law scaling (Beeson et al., 2018; Brocard and van der Beek, 2006; Langston and Temme, 2019; Langston and Tucker, 2018; May et al., 2013; Phillips, 2011; Schanz and Montgomery, 2016; Snyder et al., 2003; Tomkin et al., 2003). However, the reported range of the exponent *d* is significantly wider in valleys, ranging between negative values of -0.13 (Clubb et al., 2022) and positive values as high as~~In these cases, the reported range of the exponent *d* was significantly wider, between 0.1 (Langston and Temme, 2019) and~~ 1.18 (Beeson et al., 2018). Here too, the range was attributed to differences in the properties of the valley-bounding rocks (Brocard and van der Beek, 2006; Keen-Zebert et al., 2017; Langston and Temme, 2019; Schanz and Montgomery, 2016), or, in some high relief landscapes, to the spatial distribution of deep-seated landslides that can

cause local recession of the valley walls and, at times, dam the valley and cause upstream aggradation and widening (Beeson et al., 2018; May et al., 2013).

1.2 Width- area-slope scaling relation in channels and valleys

While the applicability of the simple ~~width-area~~ power low scaling between channel width and drainage area (Eq. (1)) was demonstrated in many settings (Montgomery and Gran, 2001; Whipple et al., 2013; Whitbread et al., 2015; Wohl and David, 2008), field observations show that it is not applicable across all landscapes. ~~Particularly~~Notably, the scaling was demonstrated to fail ~~when~~ along areas of localized gradient in rock ~~channels respond to transient conditions, such as crossing areas of enhanced~~ uplift rate ~~(~~e.g., due to local faulting or folding~~)~~ (Allen et al., 2013; Amos and Burbank, 2007; Kirby and Ouimet, 2011; Lavé and Avouac, 2001; Yanites et al., 2010), channels with alternating lithologies (Montgomery, 2004; Spotila et al., 2015), and in channels with transient morphologies due to temporal changes in rock uplift rate (Whittaker et al., 2007a, 2007b; Yanites, 2018).~~(Allen et al., 2013; Finnegan et al., 2005; Lavé and Avouac, 2001; Montgomery, 2004; Whittaker et al., 2007a; Yanites et al., 2010), inducing dynamic changes to channels local slope and width (Amos and Burbank, 2007; Kirby and Ouimet, 2011; Whipple et al., 2000; Whittaker et al., 2007a, 2007b; Yanites, 2018). Consequently, substantial research focused on understanding dynamic adjustments of bedrock channel width in response to uplift rate changes (e.g., Turowski, 2018; Wobus et al., 2006; Yanites, 2018).~~

Finnegan et al. (2005) developed a model for the case of a channel that crosses terrains with variable rock uplift rates. Adopting Manning's equation (Manning et al., 1890) and assuming a constant bankfull width-to-depth ratio along the channel, Finnegan's model predicted that the channel ~~width not only~~ depends on both the drainage area, as in Eq. (1), ~~but also on~~and the channel slope, S [m/m]:

$$W = k_b \text{~~*~~} A^b \text{~~*~~} S^c, \quad (2)$$

~~Based on theoretical calculations, t~~The exponents b and c in Finnegan's model were calculated to be ~~equal~~ 0.38 and -0.19, respectively~~. These~~, values that were later supported by observations in various ~~also validated in the~~ field studies (Finnegan et al., 2005; Kirby and Ouimet, 2011; Spotila et al., 2015; Wright et al., 2022).~~(Finnegan et al., 2005) and were later applied by following studies that examined width-area-slope scaling in field settings with alternating~~

~~lithologies and variable uplift rates (Kirby and Ouimet, 2011; Spotila et al., 2015).~~ In studies of transient channel adjustment to changing tectonic forcing, Whittaker et al. (2007a) and Attal et al. (2008) found that a greater absolute ~~studied settings of transient channels adjusting to changing tectonic forcing and suggested a more negative~~ value of -0.44 for *c* produces better fits for their field observations.~~, reflecting the dominant role of the slope in these settings.~~

The slope dependency in Eq. (2) is consistent with the approach of Turowski (2018) in scenarios where transient conditions are considered, such that the ratio of sediment flux to channel vertical erosion becomes slope dependent.

The significance of including channel slope as a controlling parameter in Eq. (2) depends on the covariance between slope and drainage area. In steady-state drainage networks with uniform lithology, climate, and uplift rates, the channel slope, *S*, and the drainage area, *A*, covary through a power-law relation $S \propto A^{-\theta}$ (Flint, 1974). Therefore, in these cases, the slope can be substituted by the drainage area, and Eq. (2) reduces to the form of Eq. (1). In contrast, the cases where Eq. (2) was found to be a better predictor for channel width (Finnegan et al., 2005; Kirby and Ouimet, 2011; Spotila et al., 2015; Whittaker et al., 2007a; Wright et al., 2022) are those where *S* and *A* do not covary, e.g., due to temporal or spatial variations in the environmental conditions.

A theory that relates valley width to drainage area and channel slope in the form of Eq. (2), was provided by Brocard and van der Beek (2006) in settings with alternating alluvial and bedrock sections. In their conceptual model, the inclusion of the channel slope, *S*, as a controlling parameter on the valley width emerges from spatial and temporal variations in the environmental conditions. For example, the channel steepness can serve as a proxy for lithological variations that set the mode of valley widening at different reaches. Alternatively, in scenarios of a channel incising into a wide flat valley, increased channel slope is often associated with bank steepening, resulting in bank slumping that forms a narrower valley within the preexisting valley bottom. Despite this appealing reasoning, to the best of our knowledge, so far Eq. (2) has not been used to predict valley width in any particular field setting.

1.~~2~~ 3 Drainage reorganization and width scaling of valleys and channels

~~Another form of variability and transiency in rivers is associated with d~~Drainage reorganization~~, which~~ is widely recognized as an important process affecting the evolution of fluvial systems (e.g., Bishop 1995, Willett et al. 2014, Fan et al., 2018; Prince et al., 2011). Reorganization occurs when drainage divides shift through time (Bishop, 1995; Davis, 1889), change basin geometry, and consequently induce changes in the discharge and drainage area

distribution along the channels (e.g., Menier et al., 2017; Pechlivanidou et al., 2019). Referring to the width-area scaling ~~The~~ scaling ~~of~~ in Eq. (1) ~~and (2) predicts that~~ the addition or reduction of drainage area ~~will result~~is expected to result in channel and valley widening or narrowing, respectively~~, of the channel and valley~~. However, ~~when~~ while drainage reorganization is capable of inducing relatively rapid drainage area changes, i.e., following river capture or repeated stochastic events (Shelef and Goren, 2021), ~~area changes via reorganization,~~ width adjustment of channels and valleys most likely requires longer time~~may not occur synchronously and can persist over long time~~ scales (Brocard and van der Beek, 2006; Wright et al., 2022) Studies that measured channel widths in drainages that experienced recent anthropogenic drainage area perturbations reported ongoing width variations that prevailed for several decades (e.g., Jones, 2018; Snyder and Kammer, 2008). Based on a theoretical model, Turowski (2020) postulated that the timescale of channel width adjustment to discharge perturbations is in the order of thousands of years. For v~~V~~alleys, the time-gap between the change in drainage area and width adjustment is expected to be even longer, most likely in the order of tens of thousands of years (Hancock and Anderson, 2002; Langston and Tucker, 2018), ~~width, particularly, is likely to adjust at slower rates than channel width~~ because it represents the channel location integrated over long periods~~, commonly in the scale of >1ky~~ (~~Hancock and Anderson, 2002; Langston and Tucker, 2018;~~ Schumm and Ethridge, 1994; Tomkin et al., 2003).

Although the potential scaling deviation following reorganization is highly consequential for fluvial landscape functionality, ~~Nonetheless, despite the intrinsic links between drainage reorganization and drainage area change, to the best of our knowledge,~~ the effect of drainage reorganization on fluvial channel and valley width scaling has not yet been evaluated. ~~Recognizing and accounting for these scaling deviations could be highly consequential for predicting the hydrologic and geomorphic functionality of reorganized drainages.~~

We hypothesize that ~~the~~ this scaling, particularly that of the valleys', expresses ~~between drainage area and width could express~~ the delayed response of width adjustment to ~~changes in~~ drainage area changes following ~~the~~ reorganization ~~of drainage networks~~. Accordingly, the coefficient and exponent values that relate drainage area with valley ~~and channel~~ width in reorganized drainages could meaningfully deviate from drainages that did not experience reorganization.

To test this hypothesis and to evaluate the effect of reorganization on the width-area ~~slope~~ scaling of valleys, we analyzed and compared the geometry of reorganized and undisturbed drainages in the southern Negev desert,

Israel, where drainage reorganization is well established by field observations (Avni et al., 2000; Ginat et al., 2000, 2002; Harel et al., 2019). In the current analysis, we aim to (~~1~~i) explore if and how the scaling between valley width~~,~~ and drainage area~~, and slope~~ in Eq. (1) varies between reorganized and non-reorganized drainages and ~~between~~ among drainages that experienced different modes of reorganization; (~~2~~ii) In cases when drainage area and slope do not covary, study the independent slope influence on valley width scaling following Eq. (2); (iii) compare the adjustment of channel width relative to valley width following reorganization; and (~~3~~iv) examine landscape evolution implications of the valley and channel width ~~area-slope~~ scaling ~~for~~ in reorganized drainages ~~on landscape evolution~~.

2. Study area

2.1 Geologic and Geomorphic setting

We explore ~~the~~ channel and valley scaling ~~between the valley and channel width, drainage area, and slope~~ along ephemeral valleys that incise into the southeastern Negev Highlands, Israel (Fig. 1). The highlands are bounded to the east by ~~The eastern boundary of the study area is the~~ ~400-600m high cliffs which rise above ~~of~~ the Arava Valley ~~(Fig. 1). The Arava Valley is a rift-like structure stretching between the Dead Sea and the Gulf of Aqaba and is the southern segment~~,part of the transtensional Dead Sea plate boundary with a rift-like structure that stretches between the Dead Sea and the Gulf of Aqaba ~~, between the Arabia plate and Sinai sub-plate~~ (Garfunkel, 1981; Garfunkel et al., 2014, Figs ~~1A~~1a-b).

The main drainage divide in the study area ~~mostly~~ separates east-flowing basins that drain across the cliff toward the Arava Valley, from west-flowing, low relief ~~channels~~ basins that flow on the Negev ~~highlands~~ Highlands (Fig. 1b-~~c~~d). The lithology exposed along the highland valleys consists primarily of Cretaceous limestone and dolomite strata (Ginat, 1991). The climate is hyper-arid with an average annual precipitation of ~<50 mm (Bitan and Rubin, 1991), typically generating one to few flashflood events per year. These climatic conditions ~~had~~ generally persisted through most of the Pleistocene (Amit et al., 2006, 2011), except for ~~relatively~~ short episodes of ~~transition to~~ wetter conditions (Ginat et al., 2018; Vaks et al., 2013).

The eastern Negev desert has been experiencing ongoing fluvial reorganization since the late Miocene (Avni et al., 2000, 2012). Before the development of the Arava Valley, rivers that originated in the Jordanian highlands, east

of the Arava Valley, flowed westward, crossing the plate boundary along the Negev highlands towards the Mediterranean (Garfunkel and Horowitz, 1966; Zilberman and Calvo, 2013). Since the Miocene, tectonic activity along the Dead Sea plate boundary formed the Arava Valley that gradually became a prominent base level. Consequently, during the Plio-Pleistocene, several large-scale capture events ~~had~~ redirected major drainage systems in the Negev toward the central Arava valley (Avni et al., 2000; Ginat et al., 2000, 2002; Guralnik et al., 2010). Field observations and a regional χ analysis (a morphometric parameter used to approximate the stability of drainage divides, (Willett et al., 2014)) suggest that the regional divide between the Arava Valley and the Negev highlands is still actively migrating westward (Harel et al., 2019).

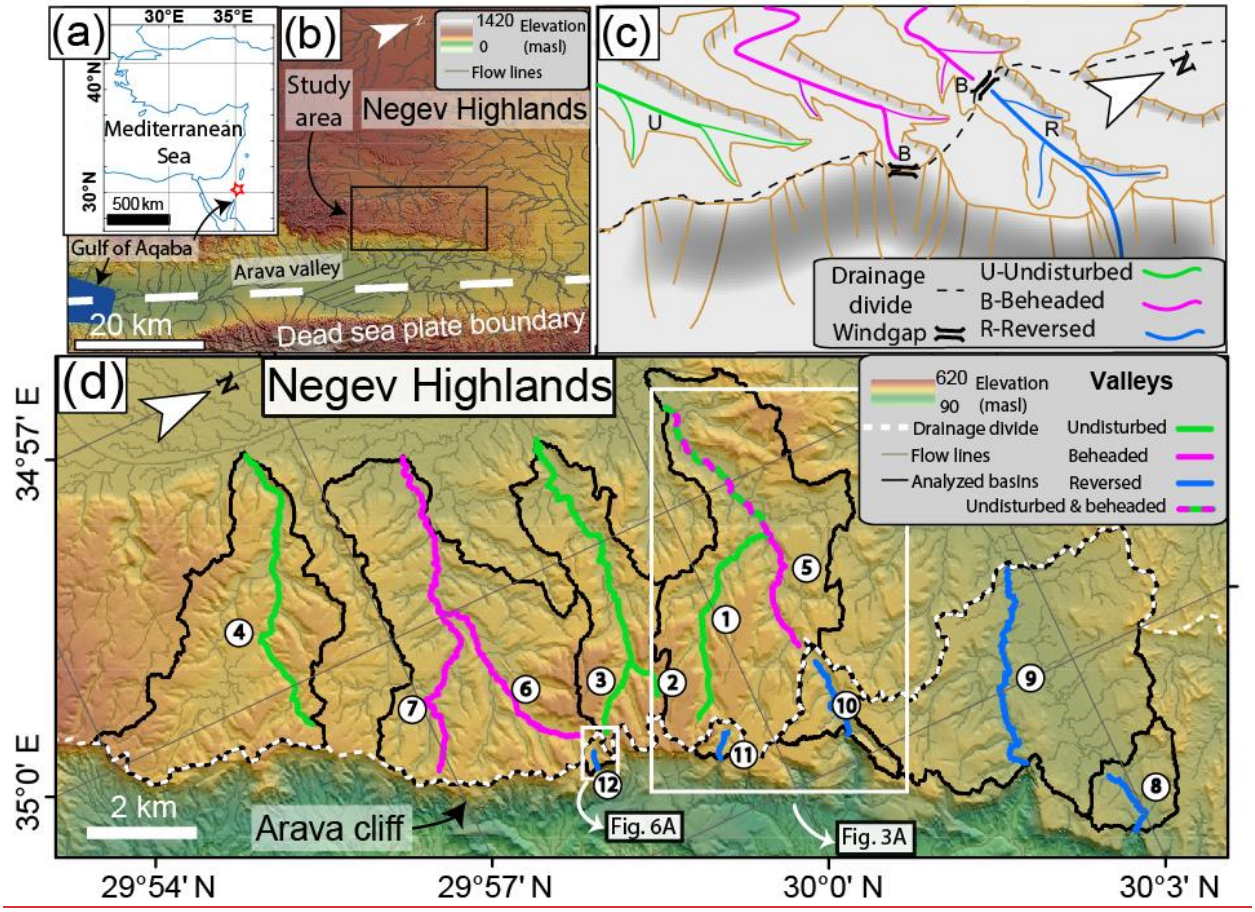

Figure 1 (a) Orientation map with coastlines (blue) showing the study area location (red star). (b) Shaded elevation map, illustrating the regional rift-morphology along the plate boundary (dashed white line) adjacent to the study area (black rectangle). The maps in (b) and (d) are based on TanDEM-X 0.4 arcsec DEM (Wessel, 2016). (c) A simplified sketch of valley categorization in the study area: Undisturbed valleys (Green, 'U' tag) are valleys that do not intersect with the cliff and are minimally affected by drainage reorganization. Beheaded valleys are valleys that were beheaded due to cliff retreat or drainage reversal (pink, ''B' tag), and Reversed valleys (blue, ''R' tag), that presently flow toward the cliff, are commonly recognized by their barbed tributaries which join the main channel at a >90 degrees angle. (d) A shaded elevation map of

the study area, illustrating the drainage divide (white dashed line) between the Negev Highlands and the Arava Valley. The basin boundaries (black lines) are defined by the valley section's outlet. Encircled numbers refer to the valley serial numbers in Tables 1 and 2.

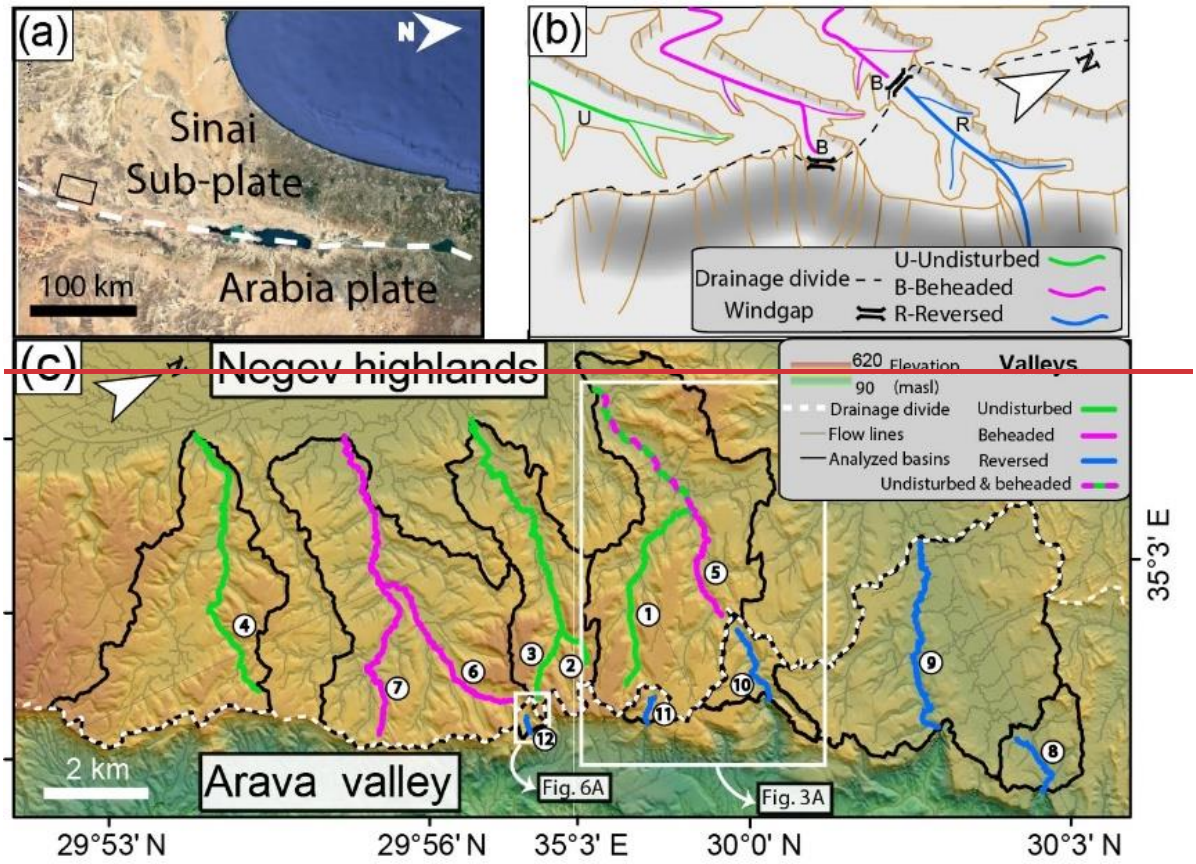

~~**Figure 1 (a) Regional map of the study area (black rectangle) near the Sinai-Arabia plate boundary (dashed white line), based on © Google earth aerial photo (2020). (b) A simplified sketch of valley categorization in the study area: Undisturbed valleys (Green, 'U' tag) are valleys that do not intersect with the cliff and are not affected by drainage reorganization. Beheaded valleys are valleys that were beheaded due to cliff retreat or drainage reversal (pink, 'B' tag), and Reversed valleys (blue, 'R' tag), that presently flow toward the cliff, are commonly recognized by their barbed tributaries which join the main channel at a >90 degrees angle. (c) Shaded elevation map of the study area, based on TanDEM-X 0.4 arcsec DEM, illustrating the drainage divide (white dashed line) between the Negev highlands and the Arava Valley. The basin boundaries (black lines) are defined by the valley section's outlet. Encircled numbers refer to the valley serial number in Table 1.**~~

2.2 Categories and characteristics of valleys in the study area

To explore the effects of drainage reorganization on the ~~scaling relations between~~valley width~~, drainage area, and slope~~ scaling relations, we analyzed 12 valley sections associated with different drainage reorganization categories.

All sections are located adjacent to the Negev-Arava drainage divide (Fig. 1d), resulting in relatively small drainage areas of 0.2-14.2 km^2. The valleys are incised into bedrock, generating ~~a~~ relief of several tens of meters between the valley bottoms and the highlands' flat interfluves. The valleys were classified into three categories, based on the association of the valley to the Arava cliff (Fig. ~~1b~~1c-~~c~~d), the morphology of the valley section (Fig. 2), and additional supporting field observations. The three categories are:

1. **Undisturbed valleys (n=4)** are westward flowing sections whose headwaters are adjacent to the cliff line and are not meaningfully beheaded. In some cases, field evidence indicates that some portions of the drainage area along the low-relief interfluves were lost due to divide migration associated with cliff receding. Yet, the receding cliff does not intersect the incised portion of the valleys; therefore, these valleys are referred to as 'undisturbed.'~~that do not show evidence of local drainage reorganization, suggesting that they were not directly affected by the formation of the Arava base level.~~ In these valleys, the low-order (sensu Strahler) incised segments are characterized by a V-shaped morphology (Figs. ~~2A~~ 2a and ~~2C~~2c) with a bedrock valley bottom that is several meters wide. Farther downstream, typically at a distance less than 1 km from the valley head, the valley bed becomes alluviated, and its width increases to tens of meters. ~~and relatively rapid downstream widening.~~ Higher-order valleys widen downstream at slower rates than low-order valleys and typically have a trapezoid cross-section with a sediment-filled flat valley ~~bed~~bottom and steep valley walls (Figs. 2b-d). In the undisturbed and beheaded categories (below), the entire valley is typically occupied by a low-relief, braided and dynamic channel system. Field observations of fully flooded valley bottom during large rainstorm events (Fig. 2d), suggest that the formative flow width is the entire width of the valley bottom.~~,~~ ~~whose relief is tens of cm (Figs. 2b-d). Here, the definition of valley and channel could be ambiguous because the low local relief results in braided and dynamic flow pathways, and because the entire valley is flooded during large rainstorm events (Fig. 2d).~~

2. **Beheaded valleys (n=3)** are west-flowing sections whose headwaters were beheaded. Beheading is ~~recognized~~ indicated by a windgap, i.e., a valley confined drainage divide ~~that occurs~~located along the cliff, or ~~that is~~ shared with a reversed valley (described below), indicating the truncation of an incised ~~a~~ paleo-valley that ~~was formed by a channel that used to~~likely drained a larger area. Close to the windgap, the beheaded valleys are characterized by a U-shaped cross-section (e.g., Figs ~~1b~~1c, 2e-f, 3a, and 6a), likely controlled by the concave profile of side colluvial aprons ~~concave profile~~. West and downstream from the windgap, ~~these~~ beheaded valleys become indistinguishable from the undisturbed valleys with the trapezoid-shaped cross-section. Valley's beheading is associated with either the

receding cliff and its coinciding divide, or with localized divide migration within the valley as part of a reversal process on the opposing side of the windgap (e.g., ~~Figs. 2e and 3a,~~ Bishop, 1995; Harel et al., 2019, Shelef and Goren, 2021). The beheaded valleys bear a similar valley bed morphology to the undisturbed category; thus, the formative flow width of the beheaded valleys is the entire width of the valley bottom.

3. **Reversed valleys (n=5)** host east-flowing channels that had reversed their drainage direction (Bishop, 1995) from west to east. These valleys are bounded between a windgap on the west side and a knickpoint on the east, where ~~generated~~ where the channel flows across the cliff (e.g., Figs 2e, 3a and 6a). Harel et al. (2019) identified these sections as reversed drainages based on the presence of barbed tributaries and west grading terraces that record the antecedent valley gradient, opposite to the present-day channel's drainage direction. The reversed valley sections share windgaps with beheaded valleys, indicating that they were part of the antecedent west-flowing drainage (Harel et al., 2019)~~(e.g., Fan et al., 2018)~~. The two northern reversed valleys (8 and 9 in Fig. 1d), initiate in a E-W trending strike valley which dictates a wide windgap (>500m, Ginat, 1997), whereas downstream from the divide they exhibit trapezoid cross-sections. In the ~~reversed valleys, the valley morphology near~~three other valleys, the windgap is typically U-shaped, and downstream the channel incises into the alluvial-colluvial valley fill, creating cut terraces and forming a V or box-shaped channel cross-section within the broader valley (e.g., transect d-d' in Figs. 2e-f). In most cases, close the the knickpoint where~~as~~ the ~~valley approaches the knickpoint over~~channel crosses the cliff, ~~the channel~~it incises into bedrock and the valley cross-section changes to a V-shaped morphology (e.g., transect c-c' in~~(Figs~~. 2e-f).

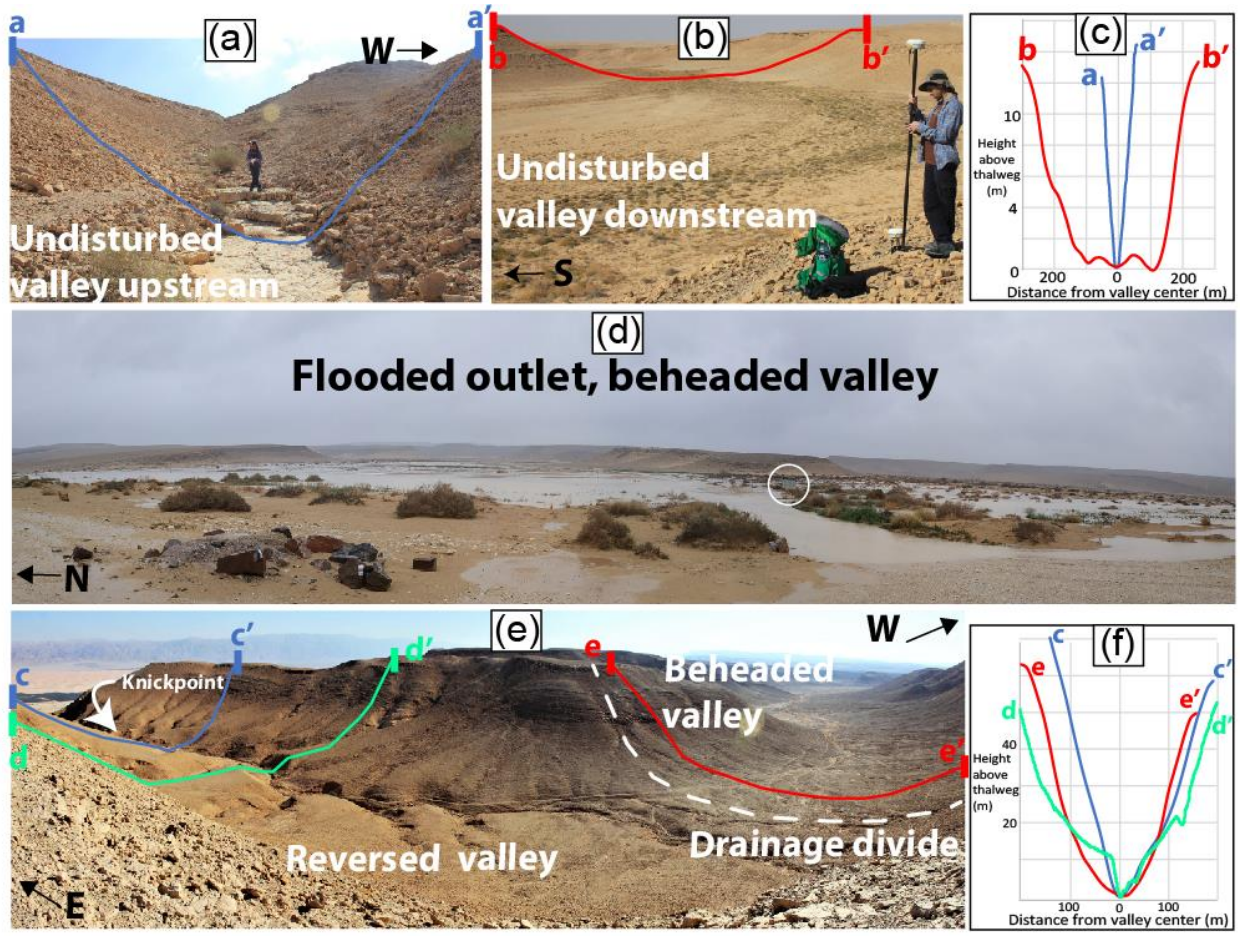

Figure 2: Field photos and valley transects of valley sections in the study area. (a,b) Upstream and downstream segments of undisturbed valleys ((a) and (b), respectively). The drainage area in panel (a) is 0.08 km^{2,} and in panel (b) is 1.85 km^{2}. Blue and red lines (a-a' and b-b,' respectively) mark the cross-section profiles shown in panel (c). (c) Transects of a-a' and b-b.' Note the V-shaped transect near the valley head relative to the trapezoid morphology of the downstream section. (d) Flooded valley bottom at the outlet of two beheaded valleys, 6 and 7, after an intense rain event in February 2020. An ~1.5 meter wide sign is encircled for scale. (e) Panorama of reversed and beheaded valleys (valley 12 and 6 in Table 1 and Fig. 1d), and the confined, flat windgap between them. The c-c' transect (blue) was measured near the knickpoint at the edge of the reversed section, d-d' (green) follows the terraces representing the paleo-valley and the channel that incises into them, and e-e' (red) was measured close to the windgap on the beheaded side. (f) Cross-sections of transects c-c', d-d,' and e-e,' emphasizing the difference between the U-shape transect near the windgap (e-e'), the V-shaped channel profile incised into the U-shaped valley terraces (d-d'), and the V-shaped valley transect above the knickpoint (c-c').

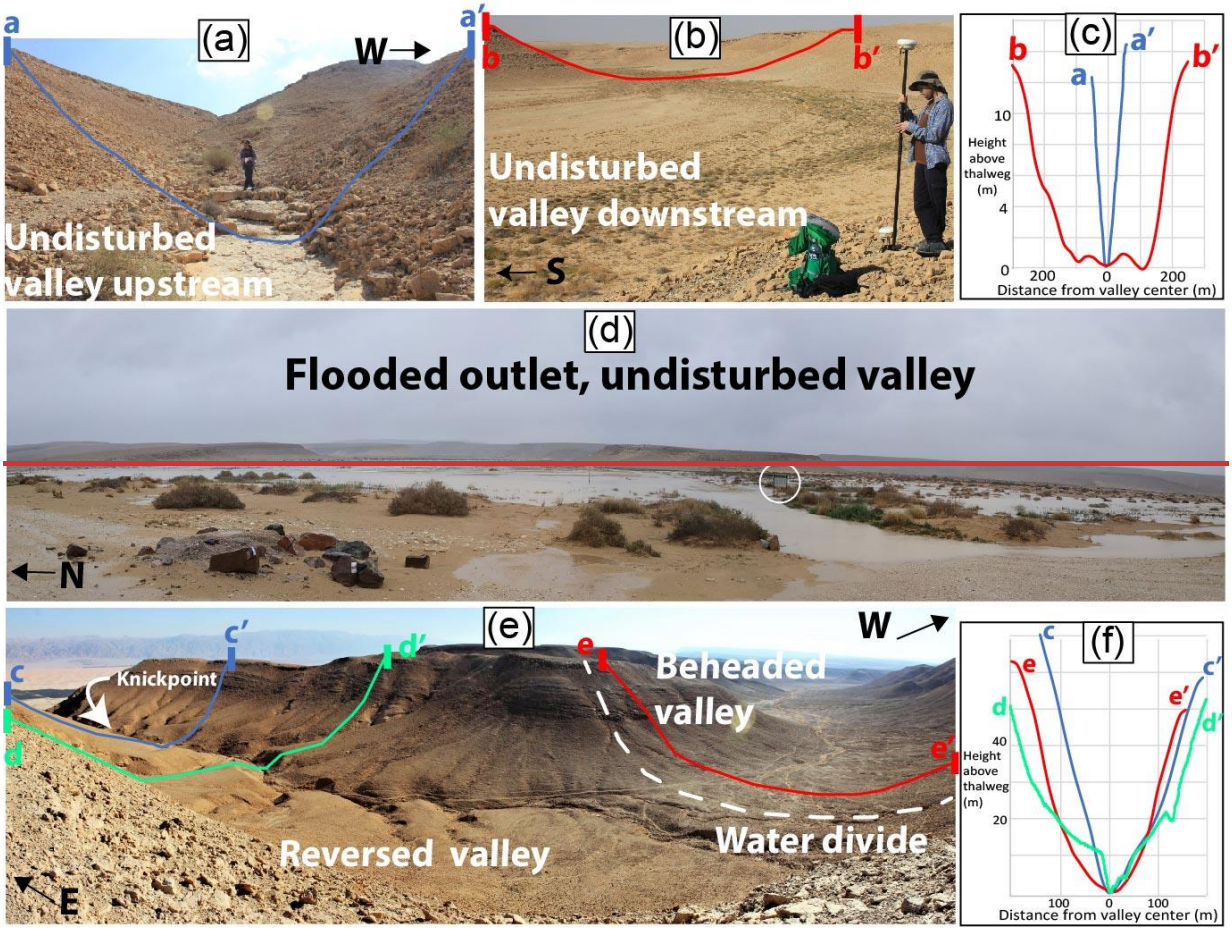

~~Figure 2: Field photos and valley transects of valley sections in the study area. (a,b) Upstream and downstream segments of undisturbed valleys ((a) and (b) respectively). The drainage area in panel (a) is 0.08 km^2, and in panel (b) is 1.85 km^2. Blue and red lines (a-a' and b-b,' respectively) mark the cross-section profiles shown in panel (c). (c) Transects of a-a' and b-b.' Note the V-shaped transect of the valley head relative to the trapezoid morphology of the downstream section. (d) Flooded valley bottom at the outlet of valleys 6 and 7, after an intense rain event in February 2020. An ~1.5 meter wide sign is encircled for scale. (e) Panorama of reversed and beheaded valleys (valley 12 and 6 in Table 1 and Fig. 1c), and the confined, flat windgap between them. The c-c' transect (blue) was measured near the knickpoint at the edge of the reversed section, d-d' (green) follows the terraces representing the paleo-valley and the channel that incises into them, and e-e' (red) was measured close to the drainage divide on the beheaded side. (f) Cross-sections of transects c-c', d-d,' and e-e' emphasizing the difference between the U-shape transect near the windgap (e-e'), the V-shaped channel profile incised into the U-shaped valley terraces (d-d'), and the V-shaped transect above the knickpoint (c-c').~~

3. Methods

We ~~study~~ studied the effect of reorganization on the ~~valley~~ width scaling of valleys by exploring the coefficients and exponents that control valley width variation, following equations (1) and (2). Valley width - drainage area scaling, based on Eq. (1), is explored for all valley sections in our study area, and the role of the slope is explored through Eq. (2) only for the reversed sections that generally show poor correlations between slope and drainage area. In one

reversed section, we focus on the scaling between channel width, drainage area and channel slope that emerge through Eq. (2).

3.1 Drainage area and slope extraction

Elevation data were derived from TanDEM-X (Wessel, 2016) with 0.4 arcsec resolution (~11.6 m/pixel in the field area). The drainage area was extracted from a flow accumulation raster, computed using a D8 flow routing algorithm (O'Callaghan and Mark, 1984). The threshold drainage areas used for defining the flow network are specified in Table S1 in the Supplement. The channel slope used for exploring slope-area relations and channel and valley width predictions following Eq. (2) was estimated along the flow network (thalweg) by using the slope of a linear regression between elevation and distance over a centered 7-pixel running window.

~~relations between valley width, drainage area, and slope following Eq. (2). While Eq. (2) was originally developed to estimate channel width, we adopt it here for valley width due to its generality. In Sect. 5.2, we devote a detailed discussion to the slope effect on valley width, which distinguishes the predictions of Eqs. (1) and (2).~~

~~To compute the coefficient k_b, and exponents b and c (Eq. (2)) that best fit the valley sections' geometry in the study area, we applied a multivariate regression over the valley width, drainage area, and slope along the studied sections. The topography data were derived from TanDEM-X DEM (Wessel, 2016) with 0.4 arcsec resolution (~11.6m in the field area).~~

~~Unlike the upstream drainage area and channel slope, which are derived by simple morphometric analysis over the DEM, defining and extracting the valley width based on DEM is not straightforward and requires a tailored procedure (Clubb et al., 2017; Golly and Turowski, 2017; Hilley et al., 2020; Roux et al., 2014; Rowland et al., 2016; Sechu et al., 2021). Particularly, the location and orientation of valley width measurements require caution because the width is not necessarily well-defined in proximity to side tributaries and valley bends (e.g., Beeson et al., 2018). To overcome these challenges, we developed a semi-automatic approach for optimal measurements of valley width.~~

3.~~1~~ 2 Valley width measurements

To compute the coefficients and exponents of Eq. (1) and (2) that best fit the geometry of valley sections in the study area, we extracted the valley widths along the analyzed valley sections. In the undisturbed and beheaded categories, the valley width refers to the flat valley bottom that is fully flooded during formative floods, while in the reversed category the valley width typically includes terraces that preserve former levels of the valley bottom (Harel et al., 2019). Unlike the upstream drainage area and slope, which are derived through relatively simple calculations over the DEM, defining and extracting the valley width based on a DEM is not straightforward and requires a tailored procedure (Clubb et al., 2017, 2022; Golly and Turowski, 2017; Hilley et al., 2020; Roux et al., 2014; Rowland et al., 2016; Sechu et al., 2021). Particularly, the location and orientation of valley width measurements require caution because the width is often not well-defined in proximity to side tributaries and valley bends (Beeson et al., 2018; Clubb et al., 2022). To overcome these challenges, we developed a semi-automatic approach for optimal measurements of valley width.

Valley width was measured by applying two consecutive ~~main~~ operations. First, a polygon representing the valley bottom ~~of drainage basins~~ is extracted, and second, valley width is measured over the valley bottom polygon at optimal points (Fig. 3a). The first step is achieved by applying the ArcGIS plugin VBET- 'Valley bottom extractor tool' (Gilbert et al., 2016). ~~In~~ VBET~~, valley boundaries are identified~~identifies valley boundaries based on user-defined slope thresholds, representing the transition from the valley bottom to the hillslope. This method particularly suites valley morphologies where the valley bottom can be easily distinguished from the valley walls based on a distinct slope break which is the case in most of the studied valley sections. VBET parameters used for the current analysis are described in Table S1 in the Supplement. Importantly, these parameters were fitted to each basin (each including one or two sections) separately by an iterative process of visually comparing the valley bottom polygons against 0.5m/pixel aerial orthophotos and fine-tuning the parameters to achieve the best visual fit. In six basins, this procedure was not sufficient to achieve a satisfying fit between the VBET polygon and the orthophoto, mainly due to local DEM inaccuracies. In these cases, the polygons were manually edited to correct mismatches. Manual editing was based on the orthophotos, available topographic data, and field observations. In five of the edited polygons, the area difference between the original and the edited polygons was < 5%;~~Except~~ in one case ~~where~~ the area difference ~~between the~~

~~original and edited polygons~~ was 10%~~, the differences in the other five basins were <5%~~ (Table S1 in the Supplement). Shapefiles of the polygons before and after manual editing are available in the Supplement.

Valley ~~Width~~ width measurements over the VBET polygons were achieved by applying an ArcGIS-based algorithm that identifies ~~optimal~~ locations for measuring valley width. that are sufficiently far from bends and confluences and are located along the valley centerline. In these optimal locations, valley transects are taken perpendicular to the centerline, whose length represents the valley width. The final output is a set of pixels located at intersections between the thalweg and the valley transects, which are assigned with valley width, drainage area, and slope values ~~The algorithm identifies points along the valley talweg that are sufficiently far from bends and confluences, such that they don't affect the valley width. The algorithm operates iteratively, where each iteration identifies optimal width measurement points in valleys of a different order. The final output of the algorithm is a set of pixels located along the intersections between the valley transects, whose length represent the valley width, and the valley talweg (flowlines)~~ (e.g., Fig 3a). The algorithm is described in detail in Section S1 and Figs. S1-S5 in the Supplement.

3.~~2~~ 3 ~~Drainage area and slope extraction, and multivariate r~~Regression analysis

~~Along the intersection pixels between width transects and the valley talweg, drainage area and slope were extracted based on the DEM. The drainage area was extracted from a flow accumulation raster, computed using a D8 flow routing algorithm (O'Callaghan and Mark, 1984). The slope was calculated using a 5 pixel running window along the channel profile, where the slope that was calculated between the terminal pixels of the window was assigned to the central pixel.~~

~~Importantly, the extracted slope is that of the channel. In the undisturbed and the beheaded valley sections, field observations indicate that the channel and the valley slope are indistinguishable (e.g., Fig. 2b,2d and 2e). This is not the case for reversed valley sections, where the channels are decoupled from the valleys. The reversed channels are incised into the bottom of paleo valleys, whose grading may be opposite to that of the active channel (Harel et al., 2019).~~

~~Direct measurements of the reversed valley's slope are unlikely to produce reliable results because the preservation of the antecedent valley bed is, in most cases, poor and patchy. In Sect. 3.3 and 5.2, we present an independent analysis dedicated to the reversed valleys and discuss the implications of using the channels' slope in the valley analysis.~~

~~After extracting the valley width, drainage area, and slope at the intersection pixels, the best-fit values of k_b, b, and c in Eq. (2) were obtained. The best-fit values were calculated by using a~~As a preliminary step to explore valley width scaling, the covariance between slope *S [m/m]* and drainage area *A [km]* was quantified using linear regression over a binned log-transformed values (e.g., Wobus et al., 2006). For all valley sections, the best-fit values of k_c and d in Eq. (1) were calculated by using a least-squares linear regression over log-transformed *W [m]* and *A [km^2]* (e.g., Fig. 3b). We used units of *[km^2]* for drainage area to facilitate direct comparison with prior studies that conducted a similar analysis using these units (e.g., Clubb et al., 2022; Langston and Temme, 2019; Schanz and Montgomery, 2016; Tomkin et al., 2003). .In the reversed category, the slope and area do not always covary, hence, in this category, we used multivariate least-squares linear regression over log – transformed *W [m]*, *A [km]*, and *S [m/m]* to find the best-fit values of k_b, b, and c in Eq. (2) (following Attal et al., 2008; Spotila et al., 2015) ~~that were log-transformed,~~ (e.g., Fig. 3~~b dc~~). In the regressions used for Eqs. (1) and (2), ~~The~~ the data points were not binned.

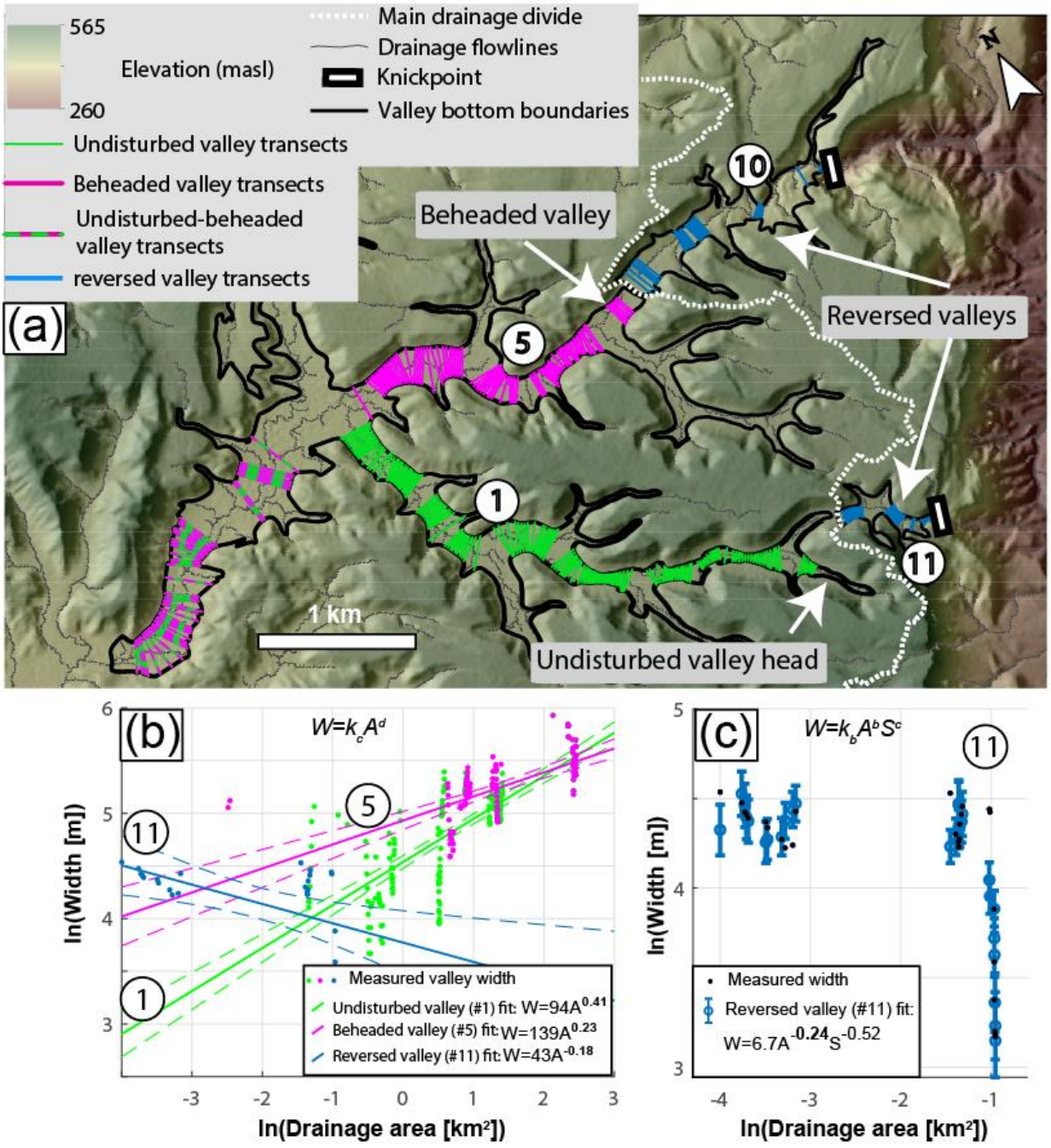

430 **Figure 3: Valley width measurements and regression-based models for valleys 1, 5, and 11 from Fig. 1d and Tables 1 and 2. (a) A valley bottom polygon (black) overlies a shaded elevation map based on TanDEM-X 0.4 arcsec DEM (Wessel, 2016). Green, pink, and blue lines represent transects of undisturbed, beheaded, and reversed valley sections, respectively. Dashed lines represent measurements at valley sections downstream of confluences between undisturbed and beheaded valleys. The reversed valleys extend between the main drainage divide (dashed white curve) and knickpoints (white boxes located at the**
435 **cliff-flowlines intersections). (b) Linear regression fitted lines from log-transformed valley width and drainage area, for the undisturbed, beheaded, and reversed valleys 1, 5, and 11, respectively. The dashed lines represent 95% confidence bounds. The equations in the bottom right are the linear models' k_c coefficients and *d* exponents. (c) Multivariate regression results with the associated k_b coefficient and *b* and *c* exponents for the reversed valley 11. The 95% confidence interval is represented by error bars.**

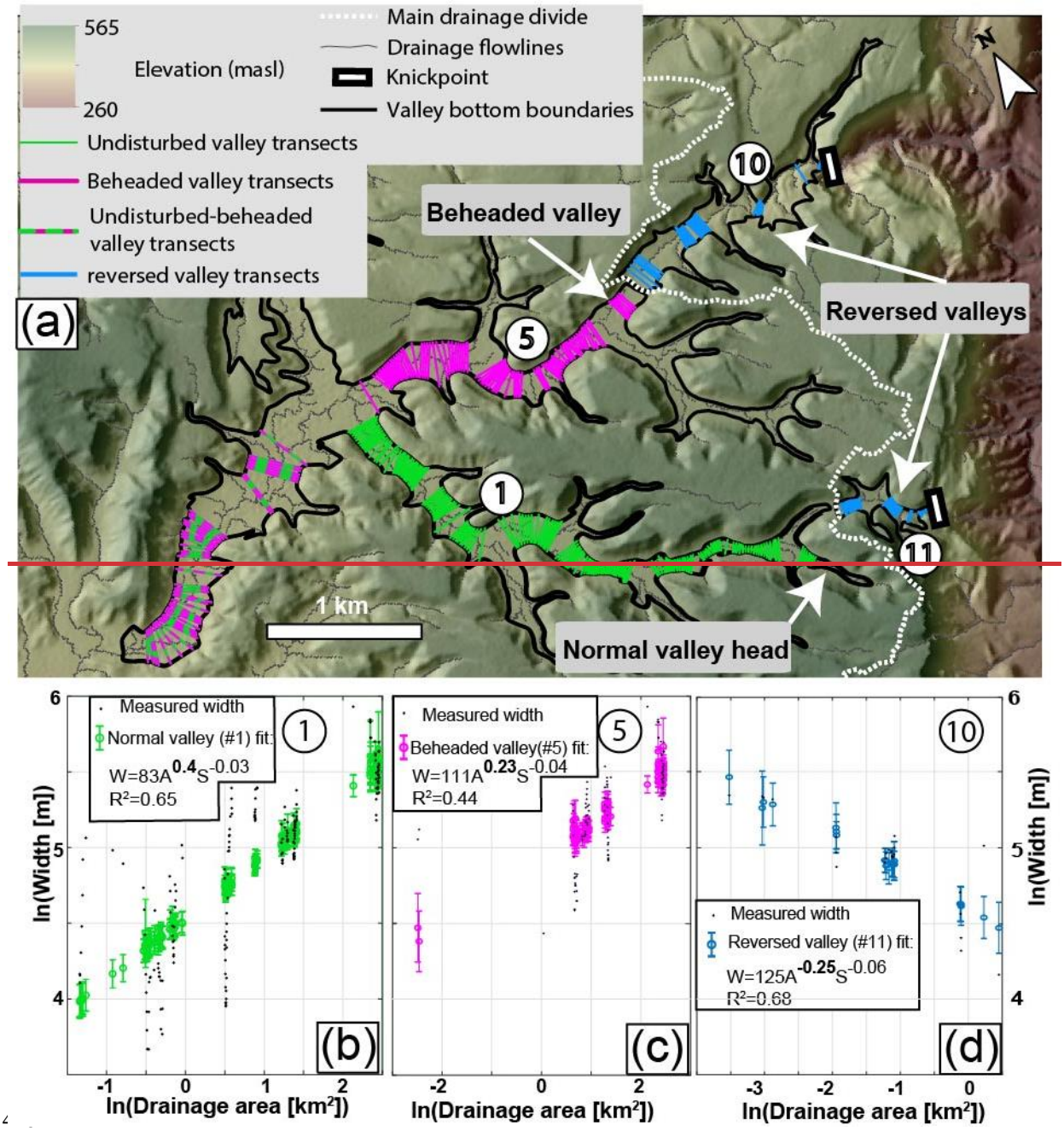

~~**Figure 3: Valley width measurements and a regression-based model for valleys 1, 5, and 10 from Fig. 1c and Table 1. (a) A valley bottom polygon (black) overlies a shaded elevation map based on TanDEM-X 0.4 arcsec DEM (Wessel, 2016). Green, pink, and blue lines represent transects of undisturbed, beheaded, and reversed valley sections, respectively. Dashed lines represent measurements at valley sections, downstream of confluences between undisturbed and beheaded valleys. The reversed valleys extend between the main drainage divide (dashed white curve) and knickpoints (white boxes located at the cliff-flowlines intersections). (b-d): Multivariate regression and the associated k_b coefficients and b and c exponents for the undisturbed, beheaded, and reversed valleys 1, 5, and 10, respectively. 95% confidence interval is represented by error bars.**~~

3.~~3~~ 4 Detailed analysis of channel and valley width

In contrast to the undisturbed and beheaded categories, in ~~For~~ the reversed category, ~~where~~ the valley and the channel are decoupled. In this category, we examined how fitting the valley width compared to the channel width affects the predictors k_b, b, and c in Eq. (2). Valley 12 (Fig. ~~1c~~ 1d and Table~~s~~ 1 and 2) is a thoroughly surveyed site ~~investigated in a previous study~~ (Harel et al., 2019) that was chosen for this analysis. The channel parameters ~~analysis is~~are based on a 15 cm/pixel DEM and a 3 cm/pixel orthophoto generated using a structure from motion (SfM) algorithm over drone-acquired aerial photos (80% overlap). Here, the sub-meter scale topography of the high-resolution DEM inhibited the VBET tool from discriminating the channel bottom precisely, and therefore the channel bottom polygon was delineated manually based on the 15 cm/pixel~~high resolution~~ DEM and orthophoto. The slope was calculated following the procedure ~~Then, the width measurement algorithm~~ described in Sect. 3.1 with a running window of 541 pixels, such that the length of the along-flow distance covered by the window was comparable to that used for the valleys. Finally, the best-fit k_b, b, and c values were calculated using a multivariate least-square linear regression ~~was applied over the channel polygon. The multivariate regressions for the channel and the valley used the slope and drainage area based on the high-resolution DEM, following the procedure~~as described in Sect. 3.~~2.~~3

3.4 Validations and errors in the measurements and model

The main potential sources of valley width measurement errors originate from the DEM horizontal resolution, R (~11.6 m^2/pixel), and the relative vertical accuracy (~2m, Wessel, 2016). To incorporate the uncertainty stemming from the horizontal resolution of the DEM, we assigned each valley width measurement with a constant error, evaluated as $\sqrt{2} * R$.

To independently explore the effect of the inaccuracies in the DEM~~vertical accuracy~~ on the final width measurements, seven valley transects ~~of seven selected sites~~ were measured with a differential GPS (DGPS). The valley bottom was extracted from the transects by applying the same slope criteria used to identify the slope-break that was applied in ~~as the~~ VBET ~~tool for~~to that basin. The DEM-based and DGPS-based valley width measurements and their relations are shown in Fig. S6 and in Table S2 in the Supplement. ~~The correspondence between the DEM and the DGPS-based width measurements is shown in Fig. 4:~~ The differences between the DEM-based ~~width~~

measurements relative to the DGPS-based measurements range between ~~1.7~~2 ~~19.8~~20 m, and are scale-independent. The percent deviation between the measurements is <0.3%, except for the narrowest valley, where ~3 m difference between the DEM and the DGPS-based measurements yielded a percent deviation of ~25%. Overall, the mean percent deviation is 3.7%, and the RMSE is 13~~.08~~ m~~,~~ (whereas the mean valley width of the seven transects is 110 m), smaller than the resolution- error of $\sqrt{2} * R$ ~~evaluated from the horizontal DEM resolution. The width measurements are available in Table S2 in the Supplement.~~

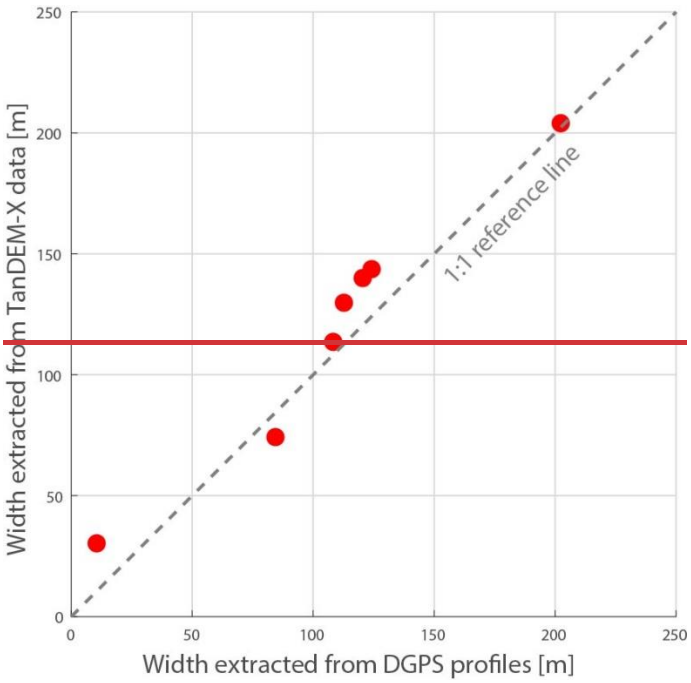

~~**Figure 4: Validation of the width measurements extracted from TanDEM-X against width measurements based on differential GPS valley transects. The maximal difference between the measurements is less than 20 m.**~~

4. Results

4.1. Slope area correlation

The slope-area relation of the studied valley sections is presented in Fig. S7 in the Supplement. The R^2 of the slope-area regressions in the undisturbed and beheaded valleys range from 0.68 to 0.93. In the reversed valleys, the R^2 of two valley sections is ~0.5, and the R^2 of the other three reversed valley sections is $R^2 < 0.14$. As mentioned in Sect. 1.2, when slope and area strongly covary, Eq. (2) reduces to the form of Eq. (1). For that reason, while the valley width – drainage area scaling (Eq. (1)) is computed for all valley categories, Eq. (2) is applied only for the reversed valley sections where the slope-area covariance is low.

4.~~1~~ 2 Valley ~~Width~~width~~, -~~ drainage area~~, and slope~~ scaling ~~along valley sections~~

The best-fit coefficients and exponents of ~~individual~~ the valley sections, their 95% confidence intervals, and the ~~adjusted~~ R^2 for the regression are presented in Table 1 and Fig. ~~5~~4. P-values of the predictors and ~~of~~ the least-square ~~multivariate~~ regressions are provided in Table S3 in the Supplement. The regressions are depicted in Fig. S8 in the Supplement.

Table 1: ~~Best fit r~~Regressions for Eq. (1), $W = k_c A^d$, all valley sections.

Valley category	Valley ID	k_c (10^{-6} $m^{(1-2d)}$), (Min.-Max 95% confidence interval)	k_c (10^{-6} m^{1-2d}) Median, (Min.-Max.)	Area exponent d, (95 % confidence interval)	d Median, (Min.-Max.)	R^2
Undisturbed	1	94, (88-99)	100, (94-110)	0.41±0.04	0.47, (0.26-0.54)	0.64
	2	106, (102-110)		0.54±0.02		0.93
	3	110, (106-113)		0.54±0.02		0.94
	4	67, (63-71)		0.26±0.04		0.45
Beheaded	5	139, (127-151)	139, (123-168)	0.23±0.05	0.18, (0.15-0.23)	0.42
	6	168, (158-177)		0.15±0.04		0.37
	7	123, (120-127)		0.18±0.02		0.73
Reversed	8	131, (95-182)	101, (24-1378),	-0.74±0.45	-0.56, (-1 - (-0.18))	0.37
	9	1378, (377-5041)		-1±0.53		0.23
	10	101, (90-113)		-0.24±0.07		0.69
	11	43, (32-59)		-0.18±0.13		0.26
	12	24, (12-49)		-0.56±0.3		0.64

Valley category	Valley ID	k_b (10^{-6} $m^{(1-2b)}$), (95% confidence interval)	k_b (10^{-6} m^{1-2b}) Range, Median	Area exponent b, (95 % confidence interval)	b Range, Median	Slope exponent c, (95 % confidence interval)	c Range, Median	Adjusted R^2
Undisturbed	1	83.09±1.29	(56.26-108.73), 95.42	0.40±0.05	(0.25-0.55), 0.47	-0.03±0.05[a]	(-0.04--0.01) -0.02	0.64
	2	108.73±1.20		0.55±0.03		0.01±0.04[a]		0.92
	3	107.75±1.16		0.53±0.03		0.01±0.03[a]		0.94
	4	56.26±1.27		0.25±0.04		-0.04±0.05[a]		0.46
Beheaded	5	111.57±1.25	(127.74-213.51), 127.74	0.23±0.05	(0.17-0.23), 0.18	-0.04±0.04	(-0.04-0.05) 0.01	0.43
	6	213.51±1.31		0.17±0.04		0.05±0.06[a]		0.38
	7	127.74±1.17		0.18±0.02		0.01±0.03[a]		0.73
Reversed	8	13.72±1.59	(3.04-125.32), 13.72	-0.33±0.19	(-0.71-(-0.24)), -0.33	-0.66±0.13	(-0.82-0.06) -0.51	0.90
	9	97.63±4.82		-0.71±0.46		-0.40±0.17		0.45
	10	125.32±1.79		-0.25±0.08		0.06±0.15[a]		0.68
	11	6.88±1.53		-0.24±0.06		-0.51±0.11		0.83
	12	3.04±3.29[a]		-0.43±0.19		-0.82±0.44		0.85

[a] Predictor P-value >0.05.

The multivariate least-square regression results reveal a unique ranges of the drainage area exponents, values, $b$$d$, for each predefined valley category (Fig. 5b4b). The undisturbed valleys are characterized by the highest exponents, ranging from 0.25 26 to 0.5554, whereas the b d exponents of the beheaded valleys are lower, 0.1715-0.23. Uniquely, the reversed valleys have negative b d exponents, ranging from -0.24 18 to -0.71, indicating that in this category, the valleys narrowthe valley narrows with increasing drainage area in this category.

Unlike the b d exponent values, the k_b-k_c coefficients values and the slope exponent values, c, are non-unique for the different categories (Fig 5a-4aand 5c). The values of the k_b-k_c coefficient, which represents the a valley width at A=1 $[km^2]$, ranges from 56.2694 to 108.7310 $(10^{-6} m^{1-2b2d})$ in the undisturbed valleys, which overlaps withdiffers from the range of the beheaded valleys category, 127.743 - 213.51168 $(10^{-6} m^{1-2b2d})$ (Fig 5a). The k_b-k_c coefficient values along for the reversed valleys show a large variability across three orders of magnitude ranging between 24 $(10^{-6} m^{1-2d})$ and 1378 $(10^{-6} m^{1-2d})$.cluster into two groups, three valleys with low values of 3.04-13.72 $(10^{-6} m^{1-2b})$, and two with higher values of 97.63 and 125.32, showing a similar range to the undisturbed and beheaded valleys.

In the undisturbed and beheaded valleys, the values of the slope exponent c are smaller by an order of magnitude relative to the values of the area exponent, b, and are statistically insignificant (with one exception in valley 5), at the 5 % significance level (Table 1). On the other hand, in all the reversed valleys except for valley 10, the values

~~of the *c* exponent are negative, have the same order of magnitude as the area exponent values, and are statistically significant (P-value <0.05).~~

The ~~model~~ performance of the power law model (Eq. 1) was evaluated through the value of R^2. In the undisturbed and beheaded categories, R^2 ranged between 0.37-0.94. In the reversed valleys, two valleys show R^2 values of 0.64 and 0.69, and the three other valleys exhibited lower values of 0.23-0.37 (Table 1). The *W-A* relations are statistically significant for all valleys (α=0.05, Table S3 in the Supplement). ~~was evaluated through the adjusted R^2, which was higher than 0.6 in most valleys, and overall >0.38 (Table 1, Fig. 5). The model P-value for all valleys was <0.05 (Table S3 in the Supplement).~~

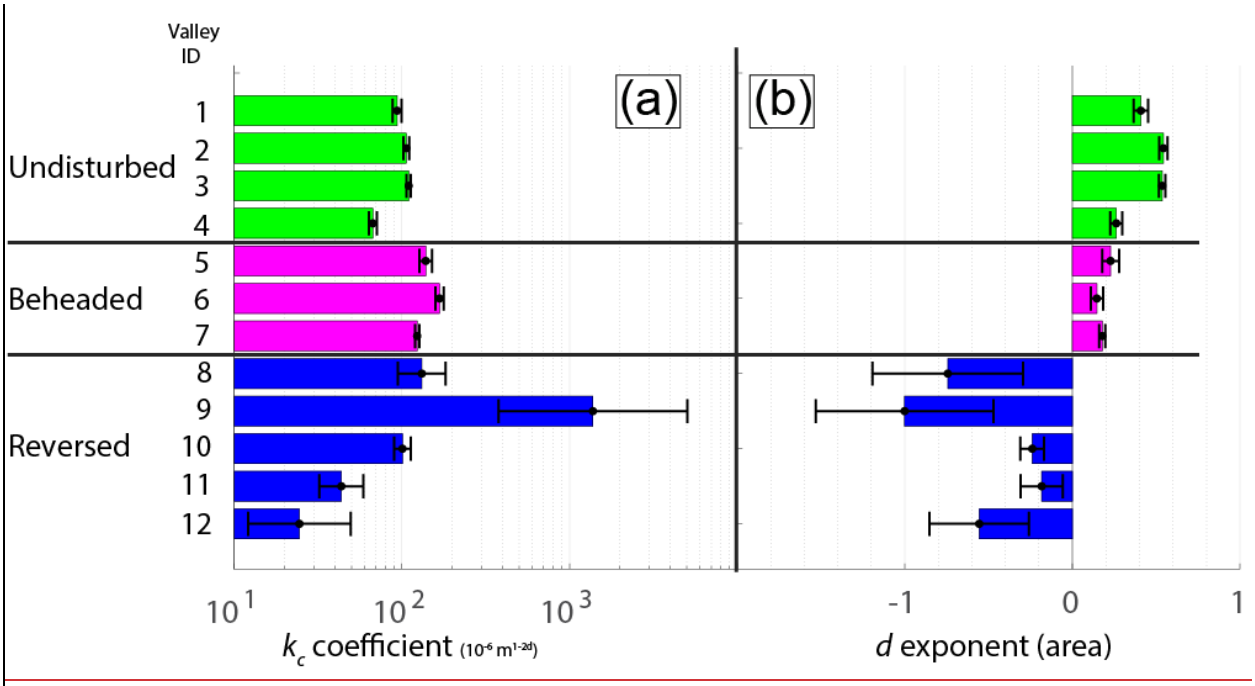

Figure 4: Bar plots of the k_c and *d* values (panels (a), (b), respectively) for valley sections of the categories defined in Fig. 1c. The error bars represent the 95% confidence interval. Unlike the k_c values, which lack a clear trend, the values of the *d* exponent (b) fall within a distinct range for each valley category. Note the log-scale of the x-axis in panel (a).

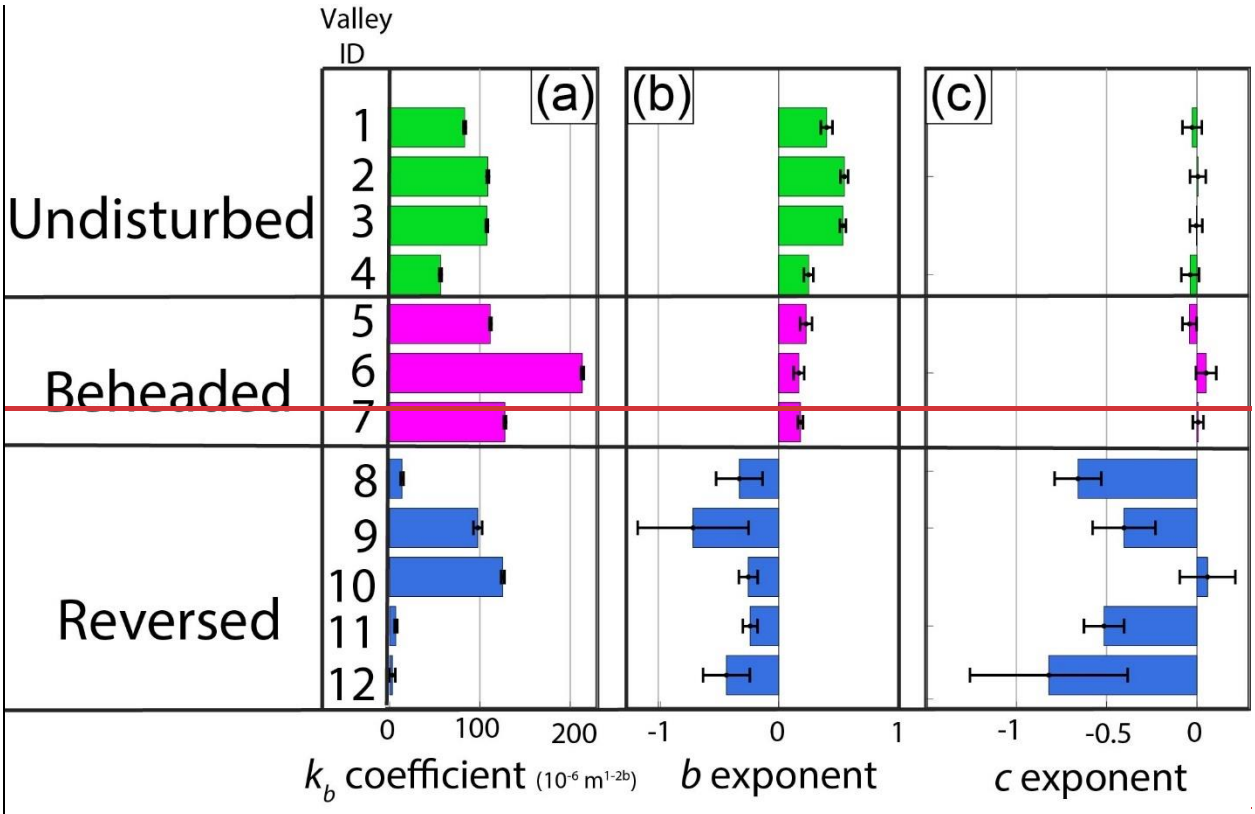

~~**Figure 5: Bar plots of the k_b, b, and c values (panels (a), (b) and (c), respectively) produced by least-square multivariate regression for valley sections of the categories defined in Fig. 1b. The error bars represent the 95% confidence interval. k_b values are generally higher in beheaded valleys, but no clear trend is observed. The most prominent trend emerges in the values of the b exponent (b), which are characterized by an exclusive range for each valley category. The values of the slope exponent, c, are approximately zero in the undisturbed and beheaded categories and mostly negative in the reversed valleys.**~~

4.3 Valley width - drainage area -slope scaling in the reversed category

The results in Sect. 4.1 demonstrate that most reversed valleys are characterized by a poor correlation between slope and drainage area. Therefore, in this category, Eq. (2) may yield a better prediction for the valley width as a function of both the drainage area and slope. In Table 2 and Fig. 5, we present the results of this multivariate regression, including 95% confidence intervals and adjusted R^2. P-values of the predictors and of the multivariate regressions are provided in Table S4 in the Supplement.

Table 2: Regressions for Eq. (2), $= k_b A^b S^c$ for reversed valley sections.

Valley category	Valley ID	k_b (10^{-6} $m^{(1-2b)}$), (Min.-Max 95% confidence interval)	k_b (10^{-6} m^{1-2b}) Median, (Min.-Max.)	Area exponent b, (95 % confidence interval)	b Median, (Min.-Max.)	Slope exponent c, (95 % confidence interval)	c Median, (Min.-Max.)	Adjusted R^2 [a]
Reversed	8	14, (9-23)	14, (2-561)	-0.32±0.21	-0.32, ((-0.98)-(-0.23)),	-0.66±0.14	-0.51, ((-0.91)-0.05)	0.89
	9	561, (146-2151)		-0.98±0.49		-0.16±0.11		0.33
	10	125, (100-155)		-0.23±0.06		0.05±0.04		0.74
	11	7, (4-10)		-0.24±0.06		-0.52±0.12		0.82
	12	2, (1-6) [b]		-0.43±0.16		-0.91±0.37		0.92

[a] Adjusted R^2 is used here for conservativeness

[b] Predictor P-value >0.05. See Table S4 in the Supplement.

The results of the multivariate regression based on Eq. (2) demonstrate that in the reversed valley sections, the drainage area exponent, b, remains negative and is within the range of -0.98 to -0.23, similar to the drainage area exponent, d computed based on Eq. (1) (Fig. 5b). The k_b coefficients are between 2 and 561 (10^{-6} m^{1-2b}) (Fig. 5a). The values of the slope exponent, c, are negative, between -0.91 and -0.16, except for valley 10, where the exponent is about zero (Fig. 5c). With the exception of valley 9, the adjusted R^2 of the model is between 0.74-0.92. Overall, all the adjusted R^2 values based on Eq. (2) are higher than the standard R^2 obtained based on Eq. (1).

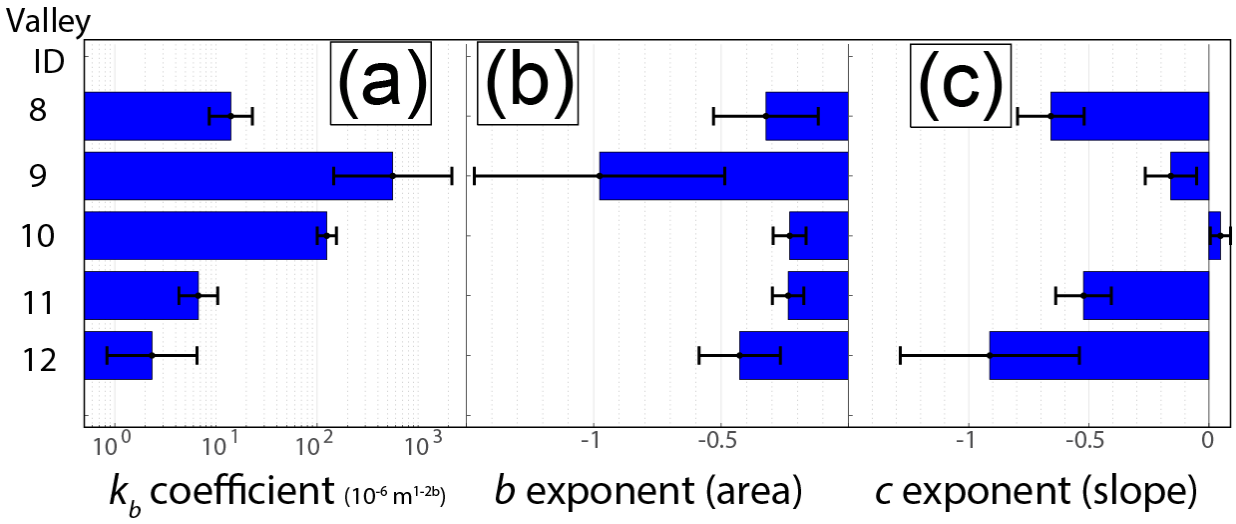

Figure 5: Bar plots of the k_b coefficient and b and c exponents in Eq. (2) for the reversed valley category (panels (a), (b), and

(c) respectively), fitted by multivariate regression. Error bars represent the 95% confidence interval. The k_b values show a large variability. The area exponents, *b*, are generally less negative than the *d* exponents fitted to Eq. (1) in Table (1) and Fig. (4). Except for valley 10, the slope exponents *c* have negative values. In valleys 8, 11, and 12, the *c* exponent is more negative than the area exponent, *b*, reflecting the key role of slope in reversed valley width prediction. Note the log-scale of the x-axis in panel (a).

4.~~2~~ 4 Comparing valley width and channel width in a reversed drainage

To~~We~~ explore~~d~~ the effect of drainage area and slope on the width of the channel vs. the width of the valley in a reversed valley section, where the valley and the channel are decoupled, we extracted the predictors k_b, *b*, and *c* in Eq. (2) for channel width in the ~~using a drone-derived high-resolution DEM of~~ reversed valley 12 (Table 1, Fig. 6). ~~Unlike the undisturbed and beheaded valley categories, the channels in the reversed settings are incised into the valley fill (Harel et al., 2019).~~ The channel in valley 12 initiates east of the windgap and incises into the erodible valley fill, where it merges with short side tributaries ~~that drain the valley bottom~~. ~~Further~~ Farther downstream, it merges with a barbed tributary that joins the valley from the north (Fig. 6a). At the barbed tributary junction point, the reversed channel is incised ~15 m below the surface of the antecedent valley bottom.~~, and after ~~ Approximately 160 m, farther downstream, bedrock is exposed at the base and the north bank of the channel. ~~At this point, the reversed channel is incised ~20 m below the surfaces of the antecedent valley bottom.~~ The channel ~~then continues for additional~~ traverses the escarpment ~~~~40 m ~~until it traverses the escarpment across~~where it forms a steep knickpoint that marks the edge of the reversed section.

Field observations show that while the reversed valley narrows downstream (i.e., eastward), the channel width increases in the ~~downstream~~is direction (Fig. 6a) , a pattern that was observed also in other reversed valley sections. In valley 12, A multivariate regression over the channel data reveals a drastically different dependency between the channel's width, drainage area, and slope compared to the valley (Fig 6b). For the channel, the least-square multivariate regression (R^2=0.~~68~~72) yields a k_b coefficient of 8 ~~$(10^{-6} m^{1-2b})$~~, with a 95 % coefficient interval of 3-17)~~10.64±2.57 $(10^{-6} m^{1-2b})$~~, a positive and high *b* exponent of 0.~~58~~62±0.~~17~~18, and a ~~relatively small,~~ negative, statistically insignificant *c* exponent of -0.~~07~~24±0.~~18~~25. In contrast, the computed values for the valley are 2 $(10^{-6} m^{1-2b})$, with a 95 % coefficient interval of 1-6) ~~3.04±3.29 $(10^{-6} m^{1-2b})$~~ for k_b, a negative *b* exponent of -0.43±0.~~19~~16, and a statistically significant *c*, -0.~~82~~91±0.~~44~~37.

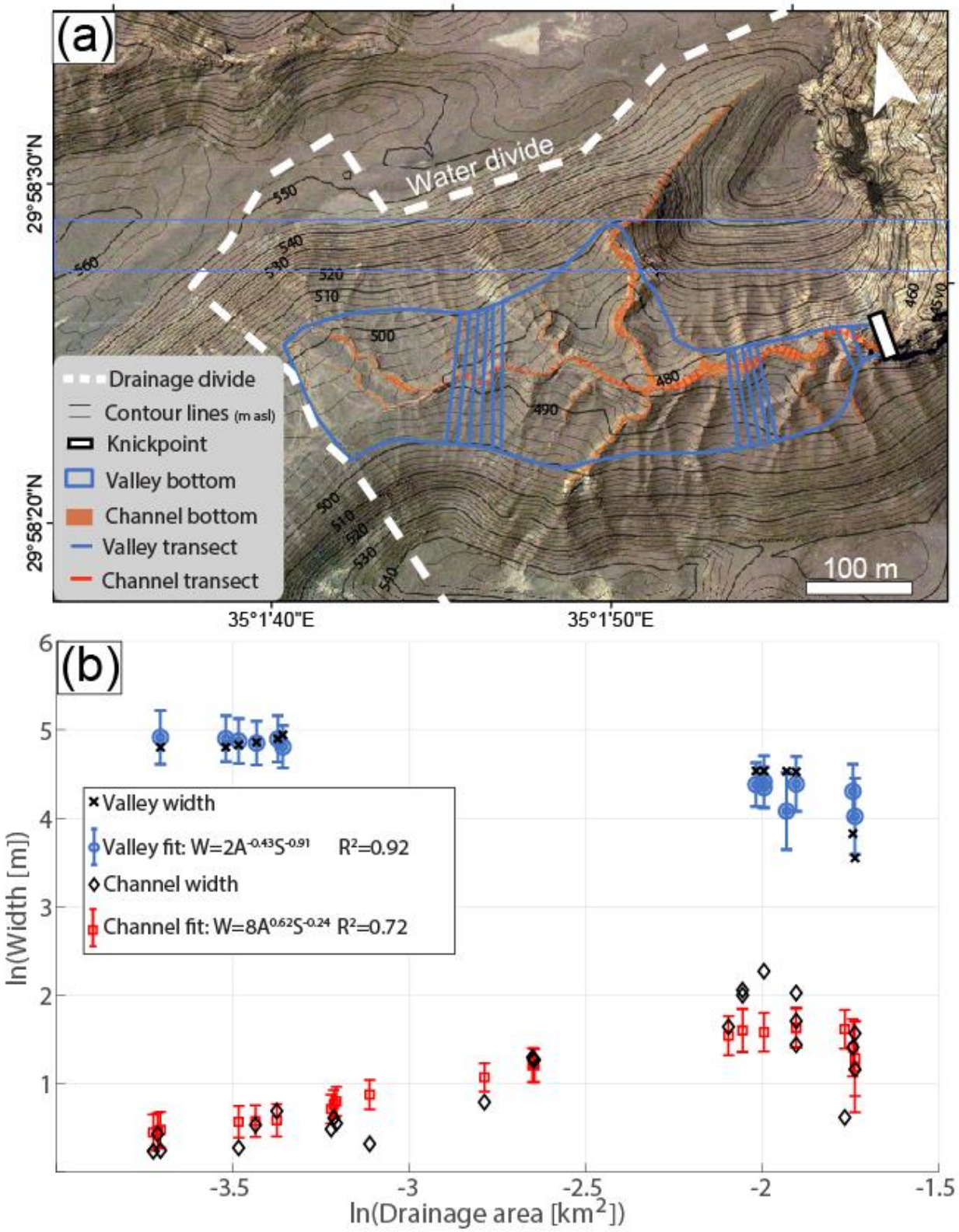
(a)
Water divide
Drainage divide
Contour lines (m asl)
Knickpoint
Valley bottom
Channel bottom
Valley transect
Channel transect
100 m
29°58'30"N
29°58'20"N
35°1'40"E
35°1'50"E
(b)
Valley width
Valley fit: W=2A^-0.43S^-0.91 R²=0.92
Channel width
Channel fit: W=8A^0.62S^-0.24 R²=0.72
ln(Width [m])
ln(Drainage area [km²])

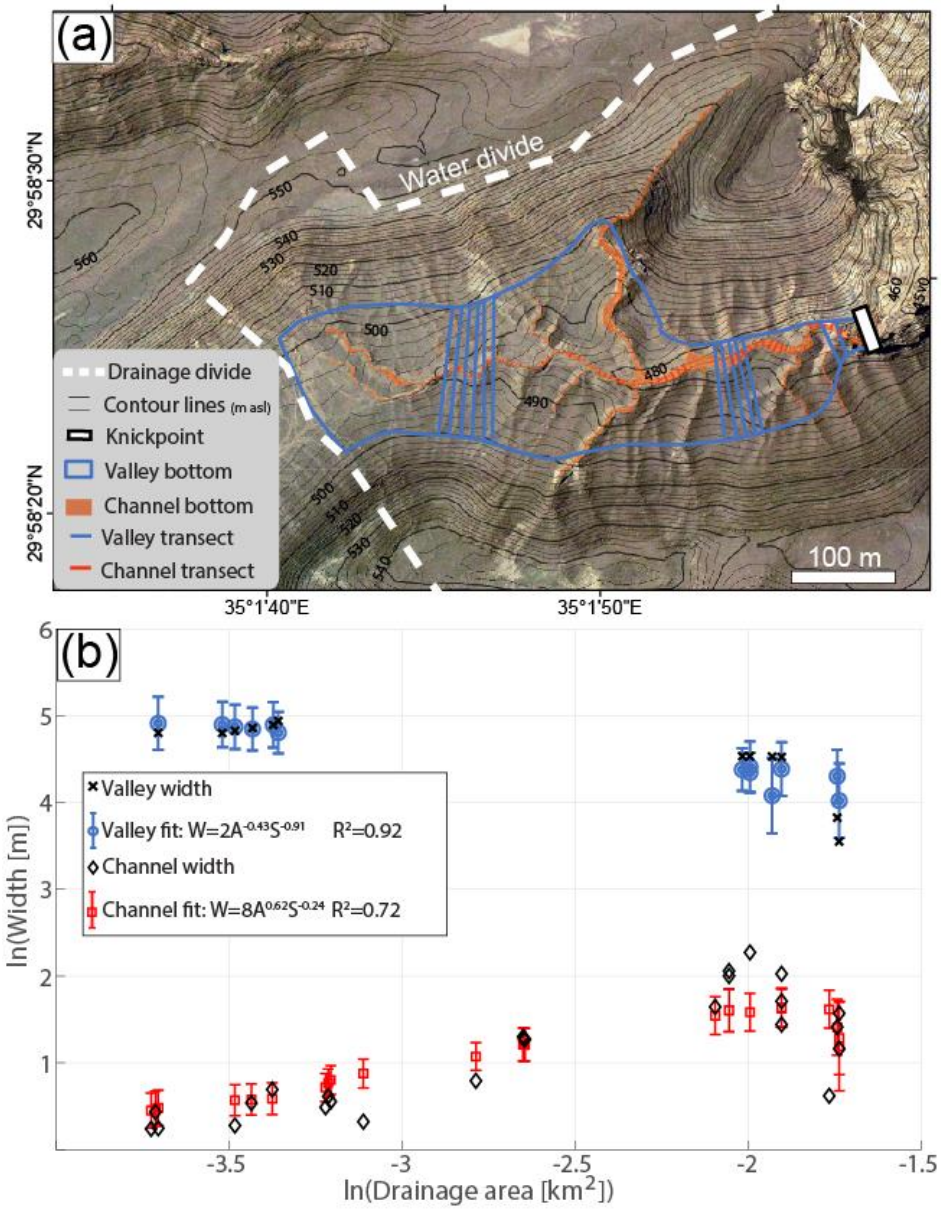

Fig 6: Variations in valley and channel widths along a reversed section (valley 12 in Tables 1 and 2, and Fig. 1d). (a) Valley (blue) and channel (orange) polygons and width transects, sketched over a 0.5 m resolution orthophoto. The slope break between the valley bottom and the hillslope is emphasized by the density change of the 2m contour lines (thin black lines). (b) Width-area-slope scaling of reversed valley width (data in black, fit in blue), which narrows with drainage area, contrasting with the width of the channel (data in black, fit in red) that increases downstream. This difference is expressed by the drainage area exponent, *b*, which is positive for the channel and negative for the valley.

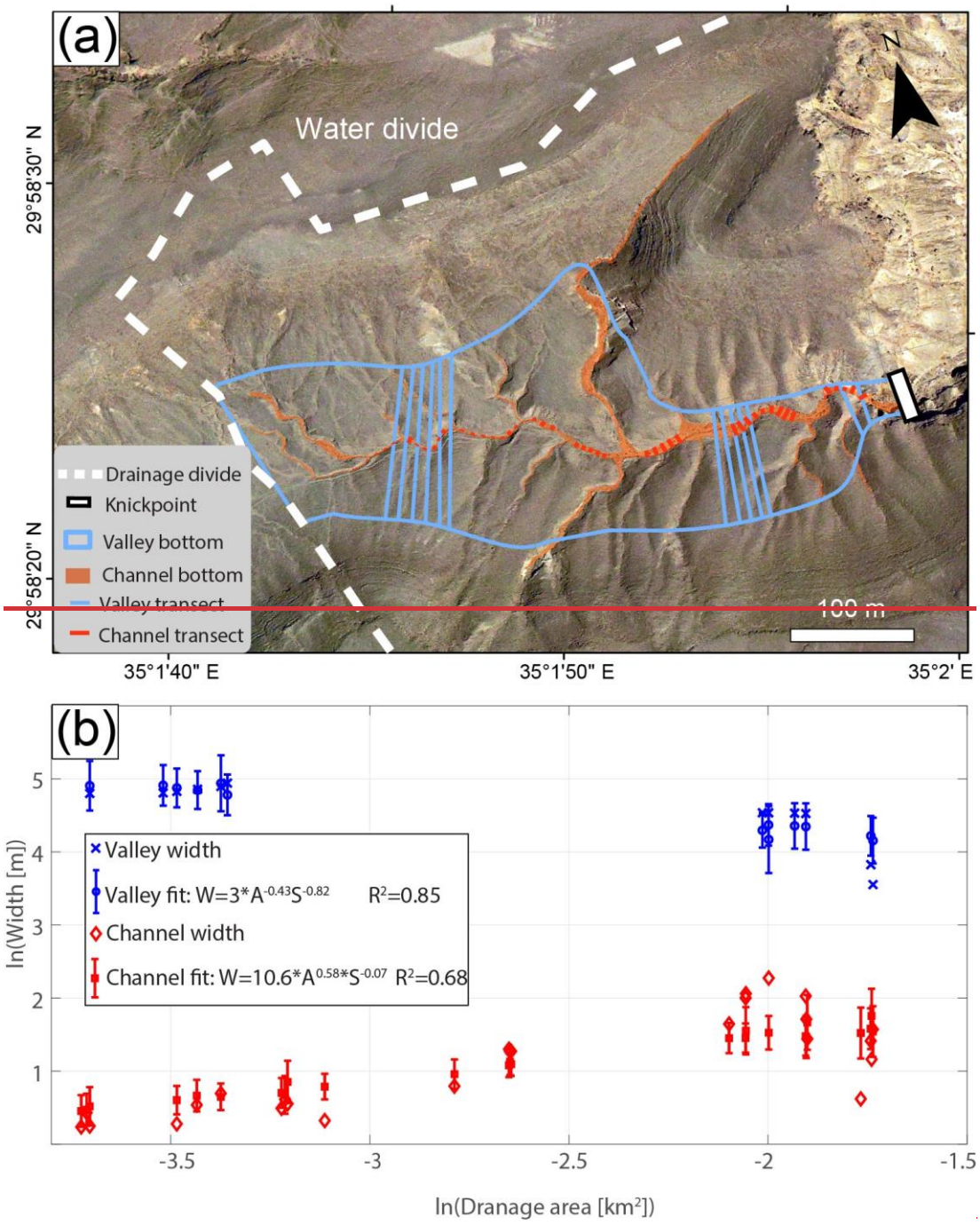

~~**Fig 6: Variations in valley and channel widths along a reversed section (valley 12 in Table 1 and Fig. 1c). (a) Valley (blue) and channel (orange) polygons and width transects sketched over a 0.5 m resolution orthophoto. (b) Width-area-slope scaling of valley width (blue), which narrows with drainage area, contrasting with the width of the reversed channel (red) that increases downstream. This difference is expressed by the drainage area exponent, *b*, which is positive for the channel and negative for the valley.**~~

5. Discussion

5.1. Drainage reorganization affects the scaling of valley width- drainage area ~~scaling~~

The ~~multivariate~~ width-area regression results reveal that undisturbed, beheaded, and reversed valleys ~~could be~~ are characterized by a distinct range of the drainage area exponent, ~~*b*~~*d*, indicating the fingerprint of reorganization in the width-area scaling of valleys.~~in the width-area slope scaling. Therefore, reorganization could meaningfully affect the width-area scaling of valleys.~~ In our study area, the ~~*b*~~ *d* exponent values of the undisturbed valleys range between 0.~~25~~ 26 and 0.~~55~~54, consistent with previously published exponent values for~~derived based on width-area or width-area slope scaling of channels and~~ valleys (Beeson et al., 2018; Brocard and van der Beek, 2006; Clubb et al., 2022; Langston and Temme, 2019; Schanz and Montgomery, 2016; Shepherd et al., 2013; Snyder et al., 2003; Tomkin et al., 2003).~~(Kirby and Ouimet, 2016; Spotila et al., 2015; Whittaker et al., 2007a, Beeson et al., 2018; Brocard and van der Beek, 2006; Langston and Temme, 2019; May et al., 2013; Schanz and Montgomery, 2016; Snyder et al., 2003; Tomkin et al., 2003).~~ The beheaded valleys in the study area are characterized by ~~*b*~~ *d* exponent values of 0.~~17~~15-0.23. While this range partly overlaps with previously published valley width-area scaling (Beeson et al., 2018;~~-~~ Clubb et al., 2022;Langston and Temme, 2019; Schanz and Montgomery, 2016), it does not overlap with the *b* exponents values of the undisturbed valleys in our study area. The low~~er~~ value~~s~~ of the ~~*b*~~ *d* exponent of the beheaded valleys, reflect~~ing~~ a smaller ~~change~~ increase of valley width *(log(W [m]))* per unit change in drainage area *(log(A [km^2]))* that~~,~~ is consistent with the process of beheading. During beheading, a valley loses its narrowest headwater sections, and consequently, the beheaded valley is wider at smaller drainage areas compared to undisturbed valleys (e.g., Fig. ~~3c~~3b). Farther downstream, as drainage area increases through contribution from non-beheaded side tributaries, the effect of beheading on drainage area decreases and the valley width – area values become similar to those of undisturbed valleys (e.g., Fig. 3a-b). Additionally, the drainage area loss reduces the discharge and sediment transport capacity near the divide and may lead to aggradation, further widening the valley bottom (Brocard and van der Beek, 2006; Langston and Tucker, 2018) in small drainage areas.~~ that widens the valley.~~ ~~Thus~~These effects act to lower~~,~~ the slope of the *log*(*W [m]*) vs. *log*(*A [km^2]*)~~ relations for~~regression line of beheaded valleys ~~are characterized by a decreased slope~~ compared to undisturbed valleys (e.g., Fig. 3b~~-c~~).

The process described above ~~is expected to also affect~~also increases the value of the ~~k_b~~ k_c coefficient values of ~~the~~ beheaded valleys compared to undisturbed valleys. However, ~~Whereas~~ whereas the median ~~k_b~~ k_c value and the

overall k_c range are ~~is~~ indeed ~~somewhat~~ higher ~~for~~ in ~~beheaded valleys compared to undisturbed ones~~ (Fig. ~~5~~ 4 and Table 1), the k_c difference i~~n~~s relatively ~~k_b is~~ small. The reason is likely that the~~his is because the value of the k_b~~ k_c coefficient reflects the valley width at a drainage area of 1 km^2 ~~(given that the c exponent is approximately zero)~~. In the study area, a 1 km^2 drainage area is reached only after the beheaded section is joined by several undisturbed tributaries, which ~~likely~~ obscures the beheading influence, and blurs the difference in k_c coefficient among the undisturbed and beheaded valleys. ~~making the k_b coefficient of the undisturbed and beheaded valleys overall similar.~~

The negative value of the ~~b~~ d exponent of the reversed valleys (between -0.~~24~~18 and -~~0.7~~1) ~~represents~~ reflects downstream valley narrowing, supporting the inferred reversal of these valley sections (Harel et al., 2019). The three southern reversed valleys (10, 11 and 12 in Tables 1 and 2 and in Fig. 1d) yield d exponents with an absolute value that is similar to that of undisturbed valley sections. This observation is consistent with the view that (i) the geometry of the antecedent valleys whose flow direction was reversed is similar to that of the undisturbed valleys (e.g., Figs 2e, 3b and 6); and (ii) valley width did not drastically change following the reversal process. The d exponents in the two northern valleys (8 and 9 in Tables 1 and 2 and in Fig. 1d) have higher absolute values, reflecting strong contrast between the narrow widths close to the knickpoint (several meters) and the anomalously high widths near the windgap (>500m), that are likely associated with the E-W trending strike valley that accommodates the windgaps. ~~Furthermore, the similar magnitude of the b exponent values (i.e., regardless of sign) for the reversed and undisturbed valley sections is consistent with the view that (1) the geometry of the undisturbed valleys is similar to the antecedent valleys whose flow direction was later reversed (e.g., Figs 2e, 3d and 6); and (2) valley width did not drastically change following the reversal process.~~

5.2. Identifying reorganization from valley width - drainage area scaling

The distinct ranges of ~~the b d~~ exponents ~~differ between~~for the undisturbed and reorganized valley~~s, in agreement~~ categories are consistent with ~~our~~ the hypothesis that drainage reorganization modifies the scaling between valley width and drainage area. Based on these results, we suggest that scaling differences could help to identify instances of drainage reorganization and point to ~~between adjacent drainages could serve as supportive evidence for drainage reorganization. Furthermore, the value of the b exponent could relate to~~ specific categories of reorganization according to the values of inferred d exponents in these sections. ~~The value of the b exponent for beheaded valleys is expected~~

~~to be lower relative to that of undisturbed valleys. Negative *b* exponents could indicate reversed drainages, where preserved antecedent valleys narrow with increased drainage area.~~ Importantly, ~~however, the width-area scaling could vary across climates (Hancock and Anderson, 2002) and lithologies (Brocard and van der Beek, 2006; Langston and Temme, 2019; Schanz and Montgomery, 2016), and is affected by structures (Keen-Zebert et al., 2017) and landslides (Beeson et al., 2018; May et al., 2013). Thus,~~ invoking ~~*b*~~ *d* exponents to support reorganization requires comparing the suspected reorganized valley sections to undisturbed sections with similar environmental ~~and structural~~ conditions because the valley widening rate could be strongly affected by local factors. Among these factors are the lithology of the valley bed and walls (Brocard and van der Beek, 2006; Langston and Temme, 2019; Langston and Tucker, 2018; Schanz and Montgomery, 2016), the climatic and glacial history of the landscape (Chen, 2021; Clubb et al., 2022; Hancock and Anderson, 2002), and geologic structures activated by tectonic forcing (Keen-Zebert et al., 2017; Whittaker et al., 2007a). Consequently, local deviations of the *d* exponent likely indicate reorganization only when the deviation is constrained across similar lithologic, climatic, and tectonic settings. When these conditions are met, we expect that deviations of the *d* exponent can serve as an effective tool for identifying reorganized drainages, regardless of the lithology and climate conditions. ~~Additionally, accurately identifying the extent of the reorganized valley section is crucial because sections that include more than a single category might show a noisy signal, if at all.~~

5.3. Influence of channel slope on predictions of reversed valley width

Our analysis reveals that Eq. (2), which includes the local slope, yields better valley width predictions for reversed valley sections compared to Eq. (1). This is evident from the high values of adjusted R^2 for the multivariate regression and the finding that in most cases, the best-fit area and slope exponents, (*b* and *c*, respectively) are of the same order of magnitude.

While the relation between valley width, drainage area and channel slope was postulated based on theoretical considerations (Brocard and van der Beek, 2006), the specific processes by which channel slope affects valley width remained vague. We suggest that in our study area, part of the correlation between the valley width and channel slope is linked to trends seen at the downstream edge of the reversed sections, above the knickpoint, where the valley narrows and the channel incises into the bedrock and steepens (e.g., valley transects in Fig 2e-f, and Fig. S9 in the Supplement). Narrowing and steepening close to the upper lip of the knickpoint is likely associated with flow acceleration above the knickpoint (Haviv et al., 2010) that forms a juvenile narrow valley (Fig. 2f). Deeper incision

above the knickpoint may cause local bank collapse that erodes the remanent terraces of the paleo valley and establishes a narrower valley that amplifies the narrowing of reversed valleys towards the knickpoints (Fig. S9 in the Supplement) and may increase the absolute value of the exponent *d* (Eq. 1). This process likely reflects a transient response to reorganization and the onset of valley width adjustment to the new drainage direction.

~~**5.2. Slope-valley width relation in the study area**~~

~~In steady-state drainage networks with uniform lithology, climate, and uplift rates, the slope, *S*, and the drainage area, *A*, scale through the power-law $S \propto A^{-\theta}$ (Flint, 1974). In such cases, slope can be substituted for area or vice versa, such that the width in Eq. (2) becomes a function of drainage area only (i.e., Eq. (2) reduces to the form of Eq. (1)) or of slope only. In contrast, when *A* and *S* do not covary, each of them can independently influence the width scaling (Finnegan et al., 2005; Whittaker et al., 2007b). In those cases, the width predicted by Eq. (2) is expected to be more accurate than that predicted by Eq. (1).~~

~~The multivariate regression results reveal three lines of evidence indicating that the valley width is independent of the slope in the undisturbed and beheaded valley sections in the study area: (i) the slope exponent , *c*, is smaller by an order of magnitude with respect to the *b* exponent (Figure 5), (ii) the values of the exponent *c* are statistically insignificant (with the exception of valley 5), and (iii) Least square regressions following the slope-independent Eq. (1) yield similar width predictors and R^2 values as the regression based on Eq. (2) (Fig. S6 in the Supplement). However, a slope-area analysis (Fig. S7a in the Supplement) shows a low covariance between *log(S [m])* and *log(A [m])*, (R^2<0.24) in the studied valley sections, indicating that the slope-independent width predictions do not arise from such covariance. Alternatively, we suggest that the statistical insignificance of the *c* exponent in the undisturbed and beheaded valley sections stems from the scatter in the slope data (Fig. S7b in Supplement), which reduces the weight of the slope relative to drainage area in the regression. The scatter is particularly distinct due to the exceptionally low slope values in these valleys, which could be <10^{-4} [*m/m*].~~

~~As opposed to the undisturbed and beheaded valleys, in the reversed valley sections (except for valley 10), the inferred slope exponents, *c*, are statistically significant, negative, and with the same order of magnitude as the area exponent *b*. Furthermore, for these sections, the multivariate regressions based on Eq. (2) produced higher R^2 values than a slope-independent regression based on Eq. (1), indicating that the slope plays a role in predicting the reversed valley width. The slope significance could be partly explained by the somewhat reduced scatter in the slope data along~~

~~the reversed category relative to the other categories, likely due to the overall higher slopes along the reversed sections (Fig. S7c in the Supplement). However, from a geomorphological perspective, the measured channel slope is expected to be decoupled from the valley morphology, because in this category, the channel and the antecedent valley grade in opposite directions (Harel et al., 2019). We suggest that the slope significance in these valleys could be explained by inspecting the width-slope correlation close to the downstream edge of the reversed sections, just above the knickpoint, where the valley narrows and channel steepens (e.g., valley transects in Fig 2e-f, and Fig. S7c in the Supplement). Narrowing and steepening could reflect channel and valley response to flow acceleration close to the upper lip of the knickpoint (Haviv et al., 2010), forming a juvenile narrow valley on the expense of the paleo valley (Fig. 2f). The incision above the knickpoint that contributes to the correlation between channel slope and valley width at the downstream edge of most reversed sections likely reflects a transient response to reorganization and the onset of valley width adjustment to the new drainage direction and drainage area distribution.~~

Valley 10 (Tables 1 and 2 and in Fig. 1d) is an interesting exception in this context. Here, despite a ~80 m high knickpoint at the edge of the reversed section, valley narrowing above the knickpoint is not prominent, and slope increase is absent (Fig. S9 and S10 in the Supplement). ~~slope increase and valley narrowing above the knickpoint are absent.~~ The lack of incision above the knickpoint in valley 10 could imply a recent episode of knickpoint migration to its current location. Accordingly, in this case, the adjusted R2 of the multivariate regression (Eq. 2, Table 2) is only slightly higher than the standard R^2 of Eq. (1) (Table 1), and the slope exponent is distinctively low (Table 2), suggesting that in this site, the inclusion of slope does not meaningfully improve the prediction of valley width. ~~multivariate regression infers a small and statistically insignificant slope exponent (Table 1).~~

5.4 Timescales and mechanisms of valley and channel width adjustment in reversed drainages

~~5.3 Differing timescales of the valley and channel width adjustment~~

~~Channel width is recognized as a sensitive parameter that adjusts dynamically and relatively rapidly to changes in tectonic (Amos and Burbank, 2007; Attal et al., 2008; Morell et al., 2020; Yanites, 2018) and climatic (DiBiase and Whipple, 2011) conditions. Over longer timescales, the valley width, which depends on the time-integrated location of the channel, is expected to adjust to the same changes in the boundary conditions (Hancock and Anderson, 2002; Langston and Temme, 2019; Tomkin et al., 2003). Drainage reorganization changes the drainage area distribution and, like tectonic and climatic variations, induces dynamic width changes. We suggest that the comparison between~~

~~the valley and channel width in reversed valley 12 (Fig. 6)~~ The comparison between the valley and channel width patterns in reversed valley 12 (Fig. 6) reveals a distinct contrast between the valleys' negative *b* exponent, reflecting a downstream valley narrowing, and the positive *b* exponent of the channel, reflecting a downstream channel widening. We suggest that this field case demonstrates a temporal snapshot where the channel width is adjusted to the new drainage area distribution inflicted by the drainage reversal~~, whereas~~ In contrast, the valley width is not yet adjusted to the change in drainage area (Fig. 6b), consistent with the longer timescales expected for valley adjustment relative to the channel (Hancock and Anderson, 2002; Langston and Tucker, 2018).

In the reversed category, an increase in drainage area is associated with the process of gradual divide migration within the antecedent valley (Harel et al., 2019). Field observations from valley 12, show that the latest drainage area redistribution phase is set by a small avulsion in a colluvial fan that drains the northern flank of the valley close to the windgap (Fig. S11 in the Supplement). The main active flow path of this fan flows east toward the reversed section; however, an older path that drains westward toward the beheaded section is not completely abandoned and is likely active when the main flow path is flooded (Shelef and Goren, 2021). This setting reflects a recent episode of flow diversion and redistribution of discharge from the beheaded to the reversed valley. Therefore, the inferred positive and high exponent of the channel width - drainage area scaling (Fig. 6) demonstrates rapid channel adjustment, in line with previous studies that proposed rapid response of channel width to environmental changes (Amos and Burbank, 2007; Attal et al., 2008; Morell et al., 2020; Snyder and Kammer, 2008; Yanites, 2018).

In deeply incised channels, where lateral erosion is minimal and hillslope erosion is enslaved to channel incision, we suggest that the time required to erode the antecedent valley bottom, *t [kyr]*, depends on the channel's vertical incision rate E_v *[m/kyr]*, the averaged hillslope angle, $\emptyset$ *[m/m]*, and the width of the antecedent valley (*W [m]*).:

$$t = \frac{W}{2E_v}\emptyset \quad (3).$$

We apply Eq. (3) to approximate the time required for reversed valley 12 to completely erode its antecedent valley. Morphometric measurements in valley 12, based on the TanDEM-X DEM, yield a maximal valley width of 125 m near the windgap and $\emptyset \sim = 0.4$. Based on the ages of abandoned terraces along channels of similar drainage areas and climate (Enzel et al., 2012), we estimated E_v to range between 0.5 to 0.05 *m/kyr*. With these values, Eq. (3) predicts a time range of 50-500 *ky*. However, the underlying assumption of Eq. (3), that hillslopes respond instantaneously to

channel incision, is not necessarily valid in arid environments where hillslope processes are slow (Ben-Asher et al., 2017; Dunne et al., 2016). The high slopes of the terrace flanks in valley 12, exceeding 0.4 in some cases, support a delayed response of the hillslope to channel incision. We therefore suggest that the predictions of equation (3) represent a lower bound when applied to arid environments.

~~same forcing (Fig. 6b), in accordance with the longer timescale expected for valley adjustment.~~

5.~~4~~ 5 Implications to landscape evolution

Delayed valley versus channel adjustment in response to reorganization (Fig. 6) and the diverging response of valleys of different reorganization categories (Fig. ~~5~~4) ~~can~~ have ~~critical~~ important implications for landscape evolution. We explore ~~one~~ an example of such an implication by inspecting the influence of channel and valley widths adjustment on a proxy for the unit stream power ($\omega = \rho g Q S / W$ *[Watt/m]*, ρ: density, g: gravitational acceleration, Q: discharge), which is commonly used for evaluating fluvial erosion rate (e.g., Harbor, 1998; Magilligan et al., 2015). Given that ρg can be treated as a constant~~,~~ and that Q is typically proportional to drainage area, the unit stream power is ~~expected to be~~ proportional to $p_{sp} = A S / W$ *[~~L~~m]* (Whittaker et al. (2007a)). Using the width of the formative flows for W, p_{sp} is calculated to explore changes in unit stream power across the windgap between reversed valley 12 and beheaded valley 6 (Fig. 7a).

Field observations demonstrate that the formative flows of reversed valley 12 are currently confined to the narrow, actively incising channel (Figs. 2e, 6, and 7a), resulting in comparably high values of p_{sp}. In contrast, across the windgap, in beheaded valley 6, the p_{sp} values are an order of magnitude lower because here, the wide valley defines the width of the formative flows, which fully occupy the flat alluvial valley bed (Figs. 2d and 7a). This difference results in a substantial step-change in the p_{sp} values across the windgap (Fig.7b, black dots), suggesting that the windgap is unstable and likely to migrate in the direction of beheaded valley 6.

~~We therefore use p_{sp} to compare the unit stream power between a reversed and beheaded valley sections that share the same windgap and flow in opposite directions (Fig. 7a). In the reversed section, p_{sp} is comparably high because of the narrow width and the increased slope of the actively incising channel (Fig. 6a). In contrast, p_{sp} is comparably low in the beheaded section, where anastomosing, low relief channels occupy almost the entire valley bed (Figs. 2a and 2d and 7a), so that the valley width represents the effective channel width. The difference in p_{sp} between~~

~~the opposing valley sections is expressed as a distinct step-change in the p_{sp} values across the windgap (Fig.7b, black x symbols), where the p_{sp} values in the reversed section are larger by an order of magnitude relative to the beheaded section.~~

~~The differences in p_{sp} across the windgap are likely associated with the formation of the reversed section, and feeds back with the reversal process.~~

Harel et al. (2019) proposed that in this study area, ~~channel~~ valley reversal initiates and extends by gradual windgap migration along an antecedent valley. Windgap migration increases the drainage area along the reversed segment, and according to the response documented in valley 12, contributes to the incision of a narrow channel within the wider antecedent valley. Across the windgap, drainage area loss hinders incision on the beheaded side, and the formative flow remains exceptionally wide.~~Linking the windgap migration to the dynamic valley and channel adjustments, we propose that in the extending reversed section, the migrating windgap increases the drainage area above the knickpoint. This, in turn, is expected to increase the erosion rates of the reversed channel, while on the beheaded side, at the other side of the windgap, the valley is losing drainage area, and experiences reduced erosion rate and even deposition, that overall reduce the rate of channel adjustment to reorganization.~~ These differences in valley response and formative flow width contribute to the p_{sp} step-change across the windgap, and, consequently, to erosion rate differences that promote further windgap migration toward the beheaded valley. This 'width feedback' adds to the drainage area feedback (Willett et al., 2014) in facilitating ongoing windgap migration, extending the reversed segment and shrinking the beheaded segment.

Importantly, the p_{sp} values of the beheaded valley (valley 6) represent a conservative estimation. First, the flatness of the beheaded valley hints that transport-limited conditions and aggradation may dominate changes in valley bed elevation rather than vertical erosion (Brocard and van der Beek, 2006; Finnegan and Balco, 2013). Second, the limited sediment transport capacity and associated sediment aggradation over the beheaded valley bed could contribute to a relatively permeable valley fill that increases infiltration, and decreases the effective discharge per drainage area.

~~stream power across the divide can cause feedback in which divide migration promotes rapid channel width adjustment on the reversed side (whose drainage area is increasing), while on the beheaded side (whose drainage area is decreasing), adjustment is detained. This, in turn, generates a step-change in unit stream power across the windgap that could further push the windgap in the same direction. This process may be perturbed by capture of side tributaries~~

~~by the reversed section, that cause abrupt changes in drainage area and erosion rate across the windgap (Shelef and Goren, 2021).~~

The step-change in p_{sp} values across the windgap emphasizes the importance of accurate channel and valley width estimates when exploring the evolution of landscapes undergoing drainage reorganization. More specifically, when the width is approximated based on ~~Eq. (2)~~ simple width-drainage area scaling, without accounting for the influence of reorganization (e.g., green open circles in Fig. 7b), ~~on the channel width (i.e., by using the same width scaling across the windgap),~~ the aforementioned step-change in p_{sp} is not recognized (Fig. 7b, ~~blue~~ green open circles ~~dots~~) ~~.~~ , and the windgap will be wrongly assumed as stable (Fig. 7b). In contrast, p_{sp} estimations based on scaling that account for reorganization are consistent with the measured p_{sp} values (blue and pink rhombuses relative to black dots in Fig. 7b) and emphasize the erosion rate difference between the reversed and the beheaded valley sections that reflects the instability of the windgap between them.

~~Consequently, a computed difference in erosion rates across the divide would be lower and the divide will be estimated as being more stable than it actually is (Fig. 7b).~~

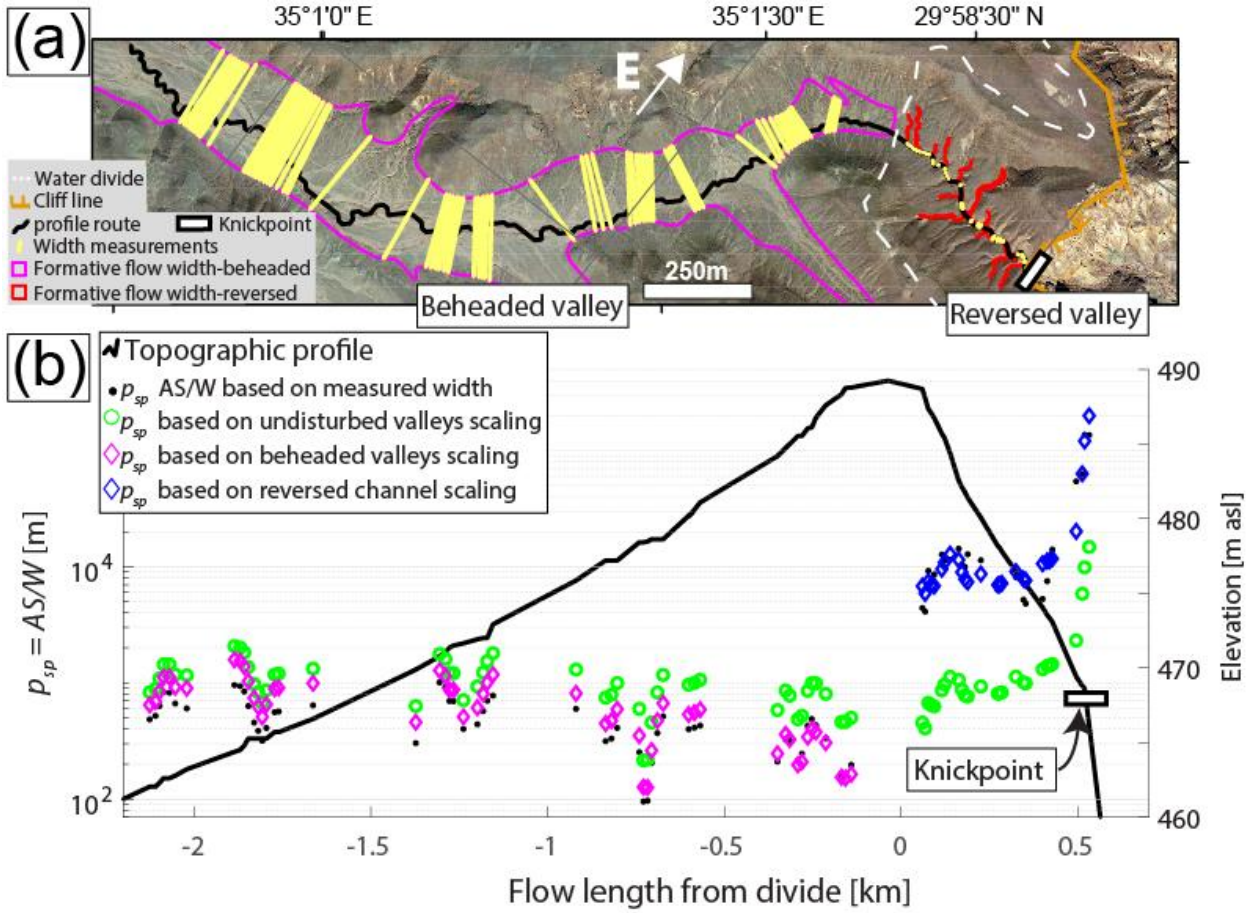

Figure 7: A proxy for unit stream power ($p_{sp}=AS/W$) along a profile from a reversed valley (# 12) to a beheaded valley (# 6) across a windgap. (a) An orthophoto of the reversed and beheaded valley sections that share a common windgap. The black line marks the profile route that follows the main channels and crosses the divide. The dashed white line marks the divide, and yellow lines mark measured width transects of the formative flow width used for calculating p_{sp}. In the reversed valley, east of the windgap, the active drainage is confined to an incised and narrow channel (Fig. 6a), whose width is used for estimating p_{sp}. West of the windgap, in the beheaded side, the formative flow width aligns with that of the valley. (b) p_{sp} estimates, based on different measurements of the formative flow width: i) Measured from DEMs (black dots), ii) Computed based on the median of the fitted predictors for undisturbed valleys in the study area, that is, without accounting for reorganization: $W=100*A^{0.47}$ (green open circles), iii) Computed based on the scaling fitted for a beheaded valley (#6 in table 1): $W=139*A^{0.18}$ (pink rhombuses) and iv) Computed based on the channel scaling for a reversed channel (Fig. 6b): $W=7.6*A^{0.62}$ (blue rhombuses). The contrast between the morphological properties of the channels in the reversed and the beheaded valleys generates a distinct step-change in the p_{sp} values across the windgap, which can promote continuous windgap migration. The trend is not predicted by p_{sp} estimations that do not account for the unique width scaling in reorganizing valleys (green open circles).

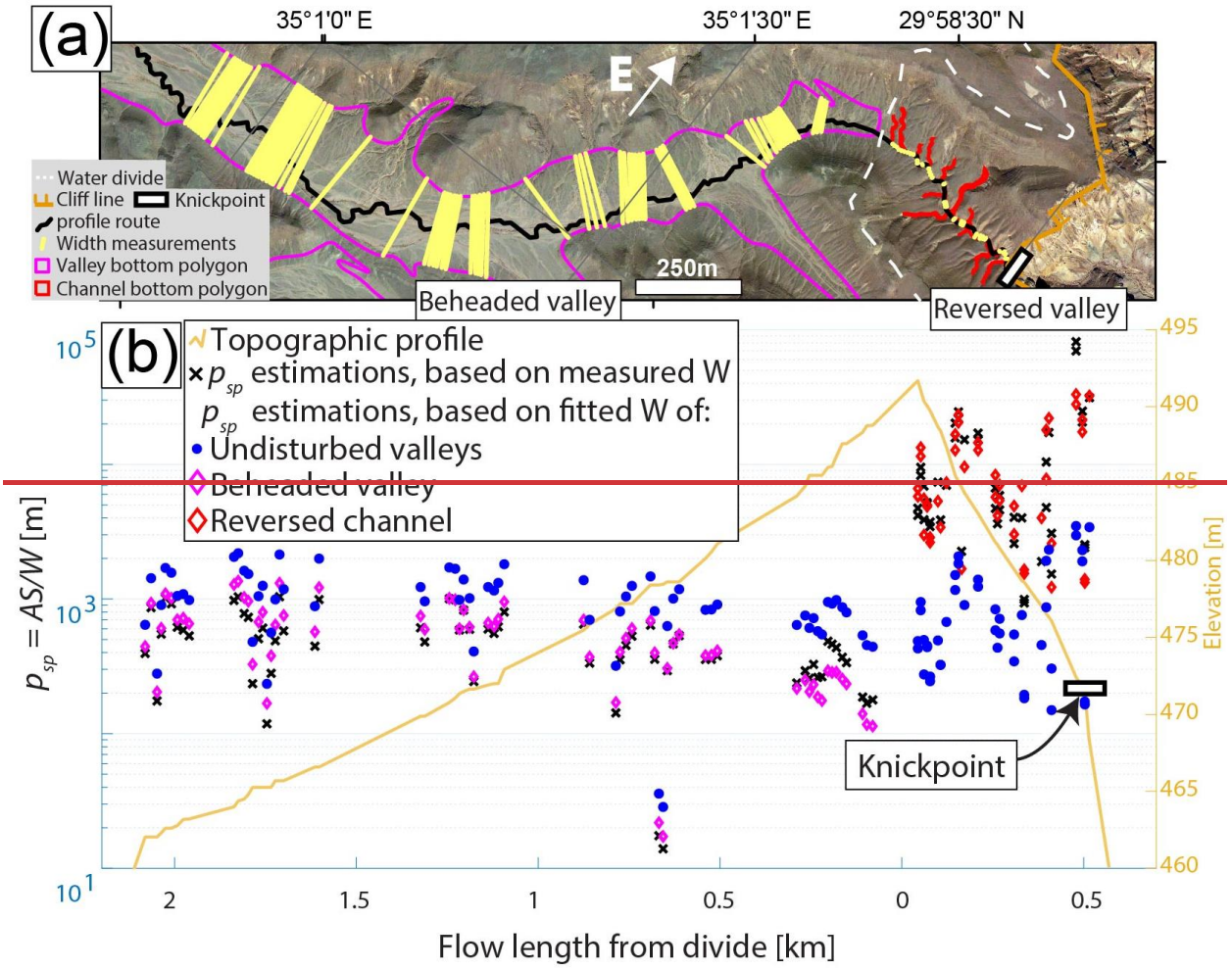

~~**Figure 7: A proxy for unit stream power ($p_{sp}=AS/W$) along a profile from a reversed valley (# 12) to a beheaded valley (# 6) across a windgap. (a) An orthophoto of the reversed and beheaded valley sections that share a common windgap. The black line marks the profile route that follows the main channels and crosses the divide. The dashed white line marks the divide, and yellow lines mark measured width transects. In the reversed valley, east of the windgap, the active drainage is confined to an incised and narrow channel (Fig. 6a), whose width is used for estimating p_{sp}. West of the windgap, in the beheaded side, the channel width aligns with that of the valley, as braided channels occupy most of the valley bed area. (b) p_{sp} estimates, based on different width measurements: i) Algorithm based, measured from DEMs (black x), ii) Computed based on the median of the fitted predictors for undisturbed valleys in the study area: $W=95*A^{0.47}S^{-0.02}$ (blue dots), iii) Computed based on *W-A-S* scaling fitted for a beheaded valley (#6 in table 1): $W=214*A^{0.17}S^{0.05}$ (pink rhombuses) and iv) Computed based on *W-A-S* channel scaling for a reversed valley (Fig. 6b): $W=10.6*A^{0.58}S^{-0.07}$ (blue rhombuses). The contrast between the morphological properties of the channels in the reversed and the beheaded valleys generate a distinct step-change in the p_{sp} values across the windgap, which can promote continuous windgap migration. The trend is not predicted by p_{sp} estimations that do not account for the unique width scaling in reorganizing valleys (blue dots).**~~

6. Conclusions

~~Our a~~Analysis of undisturbed and reorganized valley sections in the Negev desert shows that the scaling between valley width~~,~~ and drainage area ~~and slope~~ (Eq. 1) is ~~modified~~ affected by reorganization. ~~The analysis further reveals that e~~Each reorganization category is associated with a distinct range of ~~*b*~~ *d* exponent values, that ~~relating~~ relate the valley width to the drainage area. In the undisturbed valleys, the range of ~~*b*~~ *d* exponent values is overall consistent with values reported in previous studies (Attal et al., 2008; Kirby and Ouimet, 2011; Whittaker et al., 2007a). The ~~*b*~~ *d* exponent values of the beheaded valleys are positive and smaller than in undisturbed valleys. In the reversed valleys, the ~~*b*~~ *d* exponent values are negative, reflecting valley narrowing with increasing drainage area. We ~~suggest~~ propose that ~~this~~ these deviations ~~in scaling~~ could ~~be~~benefit ~~exploited, with caution, in~~ future studies that aim to identify and categorize drainage reorganization by comparing the width-area scaling of suspected reorganized drainages to those of undisturbed valleys with similar lithologic, climatic and tectonic conditions.

Most reversed valleys exhibit a poor covariance between slope and drainage area. Therefore, in this category, the valley width scaling was also inspected through Eq. 2, which incorporates both the slope and drainage area as predictors of valley width. This multivariate analysis results in higher adjusted R^2 values than those produced by Eq. (1) and resulted in negative exponents for both area and slope, (*b* anc *c*, respectively) with the same order of magnitude, indicating that they are both significant for the valley width prediction in the reversed category.

In the reversed valleys, d~~D~~ifferences in width-area-slope scaling also occur between a channel and its hosting valley. In a~~the~~ reversed valley section that we analyzed in detail, we found that the channel width is best fitted by a positive ~~*b*~~ area e~~e~~xponent *d*, whereas the exponent for the valley width is negative, reflecting a faster adjustment of channel width to the post-reorganization drainage area distribution relative to the adjustment of valley width. ~~reflecting the faster adjustment of channel width to the post-reorganization drainage area distribution relative to valley width (with a negative *b* exponent). The contrasting timescales of channel and valley width adjustment are consequential for landscape evolution.~~ Th~~is is illustrated in a~~e case study of a reversed ~~and beheaded~~ valley section that shares~~diverge from~~ a common windgap with a beheaded valley illustrates the significance of the contrasting timescales of channel and valley width adjustment for landscape evolution.. The difference between the narrow ~~width of the~~ active channel in the reversed section ~~compared to~~and the wide formative flows that occupy the entire width of the beheaded valley across the windgap ~~channel (that occupies the entire valley) of the beheaded section,~~ result~~s~~ in a step-change in unit

stream power across the windgap, used here as a proxy for fluvial erosion rate. Consequently, the step-change in unit stream power promotes divide migration and is a part of~~. Assuming that erosion rate correlates with unit stream power, this could lead to~~ a divide migration feedback~~.~~: e~~E~~rosion rate gradients across the windgap ~~promote~~ push the windgap ~~migration~~ toward the beheaded valley, which has a smaller unit stream power due to its wider channel and lower slope. Windgap migration ~~promotes~~ induces rapid channel width adjustment ~~of the channel width~~ on the extending reversed side, while on the beheaded side, adjustment is delayed, sustaining the gradient in unit stream power. This feedback suggests that the differing response of channel and valley width in different reorganization categories could ~~sustain~~ maintain ongoing divide migration, and may add to the slope and area feedbacks that were previously ~~attributed to the process~~invoked as drivers of divide migration (Plant et al., 2014; Shelef and Goren, 2021; Willett et al., 2014). This width feedback could be easily overlooked if channel width is parameterized based on standard scaling relations, which is commonly assumed in large-scale landscape evolution models (e.g., Goren et al., 2014; Lague et al., 2014; Shobe et al., 2017; Yanites et al., 2013)~~without accounting for the deviated scaling of reorganized systems.~~

Insights from this study point at several venues for future research, for example: what are the ~~timescales~~ constraints on the timescales over which the deviation in scaling persists? ~~and h~~How do they vary with climate and lithology? Could the values of the area exponents d or b ~~b~~ exponent quantify the temporal state of valley and channel adjustment ~~of channels and valleys~~? And what is the relation between the divide migration dynamics and rates to the valley and channel width adjustment?

Code and data availability

The study is based on the copyrighted 12m TanDEM-X, that is available, with service fee charge, via the link: https://tandemx-science.dlr.de/cgi-bin/wcm.pl?page=TDM-Proposal-Submission-Procedure. The data of width, slope, and drainage area of the analyzed sections , and kml shapefiles of the valley bottom polygons before and after manual editing and of the width measurements, are available at: https://doi.org/10.5281/zenodo.6970603.~~are available at: https://doi.org/10.5281/zenodo.5804837~~ . A full description of the ArcGIS model for the width measurements is found in the Supplement, and the model files are available upon request from the corresponding author.

Supplement

The Supplement related to this article is available online at: ***

Author contributions

LG and ES conceptualized the project. EH developed the software for extracting valley and channel width and performing the regression, with input from LG and ES. EH analyzed the data, generated the figures, and wrote the initial draft. LG, ES, and OC reviewed and edited the manuscript and supervised the research. HG introduced us to the field area and contributed to the ideas presented in this manuscript.

Competing interests

The contact author has declared that neither they nor their co-authors have any competing interests.

Disclaimer

Publisher's note: Copernicus Publications remains neutral with regard to jurisdictional claims in published maps and institutional affiliations.

Acknowledgements

This work is based upon work supported by the National Science Foundation – Binational Science Foundation (NSF-BSF) under Grant Numbers 1946253 (NSF), and 2019656 (BSF). We thank the German Aerospace Center (DLR) for providing the 0.4arcsec tandem-X DEM. We also acknowledge our field assistants, Eitan Meidad, Gad Reifman, Haran Henig, Omri Porat, Tom Kaner, and Yaakov Prois. Elhanan Harel thanks the Nehemia Levtzion scholarship for its support. We thank Drs. Charles Shobe, Goerge Hilley, and the anonymous reviewer for their constructive comments that significantly improved this Manuscript. Dr. Goerge Hilley suggested Eq. (3) for estimating the time required to eliminate the antecedent valley width.

References

Allen, G. H., Barnes, J. B., Pavelsky, T. M. and Kirby, E.: Lithologic and tectonic controls on bedrock channel form at the northwest Himalayan front, J. Geophys. Res. Earth Surf., 118(3), 1806–1825, doi:10.1002/jgrf.20113, 2013.

Amit, R., Enzel, Y. and Sharon, D.: Permanent Quaternary hyperaridity in the Negev, Israel, resulting from regional tectonics blocking Mediterranean frontal systems, Geology, 34(6), 509–512 [online] Available from: http://dx.doi.org/10.1130/G22354.1, 2006.

Amit, R., Simhai, O., Ayalon, A., Enzel, Y., Matmon, A., Crouvi, O., Porat, N. and McDonald, E.: Transition from arid to hyper-arid environment in the southern Levant deserts as recorded by early Pleistocene cummulic Aridisols, Quat. Sci. Rev., 30(3), 312–323, doi:https://doi.org/10.1016/j.quascirev.2010.11.007, 2011.

Amos, C. B. and Burbank, D. W.: Channel width response to differential uplift, J. Geophys. Res. Earth Surf., 112(2), 1–11, doi:10.1029/2006JF000672, 2007.

Attal, M., Tucker, G. E., Whittaker, A. C., Cowie, P. A. and Roberts, G. P.: Modelling fluvial incision and transient landscape evolution: Influence of dynamic Channel adjustment, J. Geophys. Res. Earth Surf., 113(3), 1–16, doi:10.1029/2007JF000893, 2008.

Avni, Y., Bartov, Y., Garfunkel, Z. and Ginat, H.: Evolution of the Paran drainage basin and its relation to the Plio-Pleistocene history of the Arava Rift western margin, Israel., Isr. J. Earth Sci., 49(4), 215–238, doi:10.1560/W8WL-JU3Y-KM7W-8LX4, 2000.

Avni, Y., Segev, A. and Ginat, H.: Oligocene regional denudation of the northern Afar dome: Pre- and syn-breakup stages of the Afro-Arabian plate, Bull. Geol. Soc. Am., 124(11–12), 1871–1897, doi:10.1130/B30634.1, 2012.

Beeson, H. W., Flitcroft, R. L., Fonstad, M. A. and Roering, J. J.: Deep-Seated Landslides Drive Variability in Valley Width and Increase Connectivity of Salmon Habitat in the Oregon Coast Range, JAWRA J. Am. Water Resour. Assoc., 54(6), 1325–1340, 2018.

Ben-Asher, M., Haviv, I., Roering, J. J. and Crouvi, O.: The influence of climate and microclimate (aspect) on soil creep efficiency: Cinder cone morphology and evolution along the eastern Mediterranean Golan Heights, Earth Surf. Process. Landforms, 42(15), 2649–2662, doi:https://doi.org/10.1002/esp.4214, 2017.

Bertrand, M. and Liébault, F.: Active channel width as a proxy of sediment supply from mining sites in New Caledonia, Earth Surf. Process. Landforms, 44(1), 67–76, doi:https://doi.org/10.1002/esp.4478, 2019.

Bishop, P.: Drainage rearrangement by river capture, beheading and diversion, Prog. Phys. Geogr., 19(4), 449–473, doi:10.1177/030913339501900402, 1995.

Bitan, A. and Rubin, S.: Climatic atlas of Israel for physical and environmental planning and design, Minist. Transp. Jerusalem, 1991.

Brocard, G. Y. and van der Beek, P. A.: Influence of incision rate, rock strength, and bedload supply on bedrock river gradients and valley-flat widths: Field-based evidence and calibrations from western Alpine rivers (southeast France), S. D. Willett al., Spec. Pap. Geol. Soc. Am, 398, 101–126, 2006.

Brussock, P. P., Brown, A. V and Dixon, J. C.: CHANNEL FORM AND STREAM ECOSYSTEM MODELS, JAWRA J. Am. Water Resour. Assoc., 21(5), 859–866, doi:10.1111/j.1752-1688.1985.tb00180.x, 1985.

Chen, A.: Climatic controls on drainage basin hydrology and topographic evolution, University of Bristol., 2021.

Clubb, F. J., Mudd, S. M., Milodowski, D. T., Valters, D. A., Slater, L. J., Hurst, M. D. and Limaye, A. B.: Geomorphometric delineation of floodplains and terraces from objectively defined topographic thresholds, Earth Surf. Dyn., 5(3), 369–385, doi:10.5194/esurf-5-369-2017, 2017.

Clubb, F. J., Weir, E. F. and Mudd, S. M.: Continuous measurements of valley floor width in mountainous landscapes, , (February), 1–27, 2022.

Davis, W. M.: A river-pirate, Science (80-.)., 13, 108–109, 1889.

Dunne, T. and Leopold, L. B.: Water in environmental planning, Macmillan., 1978.

Dunne, T., Malmon, D. V and Dunne, K. B. J.: Limits on the morphogenetic role of rain splash transport in hillslope evolution, J. Geophys. Res. Earth Surf., 121(3), 609–622, doi:https://doi.org/10.1002/2015JF003737, 2016.

Dury, G. H.: Principles of underfit streams, US Government Printing Office., 1964.

Enzel, Y., Amit, R., Grodek, T., Ayalon, A., Lekach, J., Porat, N., Bierman, P., Blum, J. D. and Erel, Y.: Late Quaternary weathering, erosion, and deposition in Nahal Yael, Israel: An "impact of climatic change on an arid watershed"?, Bulletin, 124(5–6), 705–722, 2012.

Fan, N., Chu, Z., Jiang, L., Hassan, M. A., Lamb, M. P. and Liu, X.: Abrupt drainage basin reorganization following a Pleistocene river capture, Nat. Commun., 9(1), 1–6, 2018.

Faustini, J. M., Kaufmann, P. R. and Herlihy, A. T.: Downstream variation in bankfull width of wadeable streams across the conterminous United States, Geomorphology, 108(3–4), 292–311, doi:10.1016/J.GEOMORPH.2009.02.005, 2009.

Finnegan, N. J. and Balco, G.: Sediment supply, base level, braiding, and bedrock river terrace formation: Arroyo Seco, California, USA, Bull. Geol. Soc. Am., 125(7–8), 1114–1124, doi:10.1130/B30727.1, 2013.

Finnegan, N. J., Roe, G., Montgomery, D. R. and Hallet, B.: Controls on the channel width of rivers: Implications for modeling fluvial incision of bedrock, Geology, 33(3), 229–232, doi:10.1130/G21171.1, 2005.

Fisher, G. B., Bookhagen, B. and Amos, C. B.: Channel planform geometry and slopes from freely available high-spatial resolution imagery and DEM fusion: Implications for channel width scalings, erosion proxies, and fluvial signatures in tectonically active landscapes, Geomorphology, 194, 46–56, doi:10.1016/j.geomorph.2013.04.011, 2013.

Flint, J. J.: Stream gradient as a function of order, magnitude, and discharge, Water Resour. Res., 10(5), 969–973, doi:10.1029/WR010i005p00969, 1974.

Fryirs, K. A., Brierley, G. J., Wheaton, J. M., Bizzi, S. and Williams, R.: To plug-in or not to plug-in ? Geomorphic analysis of rivers using the River Styles Framework in an era of big data acquisition and automation, , (June), 1–20, doi:10.1002/wat2.1372, 2019.

Garfunkel, Z.: Internal structure of the Dead Sea leaky transform (rift) in relation to plate kinematics, Tectonophysics, 80(1–4), 81–108, 1981.

Garfunkel, Z. and Horowitz, A.: The upper Tertiary and Quaternary morphology of the Negev, Israel, Isr. J. Earth Sci, 15(3), 101–117, 1966.

Garfunkel, Z., Ben-Avraham, Z. and Kagen, E.: Dead Sea Transform Fault System : Reviews., 2014.

Giaconia, F., Booth-Rea, G., Martínez-Martínez, J. M., Azañón, J. M., Pérez-Peña, J. V., Pérez-Romero, J. and Villegas, I.: Geomorphic evidence of active tectonics in the Sierra Alhamilla (eastern Betics, SE Spain), Geomorphology, 145–146, 90–106, doi:https://doi.org/10.1016/j.geomorph.2011.12.043, 2012.

Gibling, M. R.: Width and Thickness of Fluvial Channel Bodies and Valley Fills in the Geological Record: A Literature Compilation and Classification, J. Sediment. Res., 76(5), 731–770, doi:10.2110/jsr.2006.060, 2006.

Gilbert, J. T., Macfarlane, W. W. and Wheaton, J. M.: The Valley Bottom Extraction Tool (V-BET): A GIS tool for delineating valley bottoms across entire drainage networks, Comput. Geosci., 97, 1–14, doi:10.1016/j.cageo.2016.07.014, 2016.

Ginat, H.: The geology and geomorphology of Yotvata Region, Isr. Geol. Surv. Rep. GSI/8/91, 1991.

Ginat, H.: Paleogeography and the landscape evolution of the Nahal Hiyyon and Nahal Zihor basins (sedimentology, climatic and tectonic aspects). Israel Geological Survey Report GSI/19/97 (Hebrew, English abstract), Isr. Geol. Surv. Rep. GSI/19/97 (Ph. D. Diss., 206, 1997.

Ginat, H., Zilberman, E. and Avni, Y.: Tectonic and paleogeographic significance of the Edom River , a Pliocene stream that crossed the Dead Sea Rift valley, Isr. J. Earth Sci., 49(1), 159–177, doi:10.1560/N2P9-YBJ0-Q44Y-GWYN, 2000.

Ginat, H., Zilberman, E. and Amit, R.: Red sedimentary units as indicators of Early Pleistocene tectonic activity in the southern Negev desert, Israel, Geomorphology, 45(1–2), 127–146, doi:10.1016/S0169-555X(01)00193-3, 2002.

Ginat, H., Opitz, S., Ababneh, L., Faershtein, G., Lazar, M., Porat, N. and Mischke, S.: Pliocene-Pleistocene waterbodies and associated deposits in southern Israel and southern Jordan, J. Arid Environ., 148, 14–33, doi:10.1016/j.jaridenv.2017.09.007, 2018.

Golly, A. and Turowski, J. M.: Deriving principal channel metrics from bank and long-profile geometry with the R package cmgo, Earth Surf. Dyn., 5(3), 557–570, 2017.

Goren, L., Willett, S. D., Herman, F. and Braun, J.: Coupled numerical-analytical approach to landscape evolution modeling, Earth Surf. Process. Landforms, 39(4), 522–545, doi:10.1002/esp.3514, 2014.

Guralnik, B., Matmon, A., Avni, Y. and Fink, D.: 10Be exposure ages of ancient desert pavements reveal Quaternary evolution of the Dead Sea drainage basin and rift margin tilting, Earth Planet. Sci. Lett., 290(1–2), 132–141, doi:10.1016/j.epsl.2009.12.012, 2010.

Hancock, G. S. and Anderson, R. S.: Numerical modeling of fluvial strath-terrace formation in response to oscillating climate, , (9), 1131–1142, 2002.

Harbor, D. J.: Dynamic equilibrium between an active uplift and the Sevier River, Utah, J. Geol., 106(2), 181–194, 1998.

Harel, E., Goren, L., Shelef, E. and Ginat, H.: Drainage reversal toward cliffs induced by lateral lithologic differences, Geology, 2019.

Haviv, I., Enzel, Y., Whipple, K. X., Zilberman, E., Matmon, A., Stone, J. and Fifield, K. L.: Evolution of vertical knickpoints (waterfalls) with resistant caprock: Insights from numerical modeling, J. Geophys. Res. Earth Surf., 115(F3), doi:https://doi.org/10.1029/2008JF001187, 2010.

Hilley, G. E., Baden, C. W., Dobbs, S. C., Plante, Z., Sare, R. and Steelquist, A. T.: A Curvature-Based Method for

Measuring Valley Width Applied to Glacial and Fluvial Landscapes, J. Geophys. Res. Earth Surf., 125(12), e2020JF005605, doi:https://doi.org/10.1029/2020JF005605, 2020.

Jones, J. C.: Historical channel change caused by a century of flow alteration on Sixth Water Creek and Diamond Fork River, UT, Utah State University., 2018.

Keen-Zebert, A., Hudson, M. R., Shepherd, S. L. and Thaler, E. A.: The effect of lithology on valley width, terrace distribution, and bedload provenance in a tectonically stable catchment with flat-lying stratigraphy, Earth Surf. Process. Landforms, 42(10), 1573–1587, doi:10.1002/esp.4116, 2017.

Kirby, E. and Ouimet, W.: Tectonic geomorphology along the eastern margin of Tibet: Insights into the pattern and processes of active deformation adjacent to the Sichuan Basin, Geol. Soc. Spec. Publ., 353, 165–188, doi:10.1144/SP353.9, 2011.

Lague, D.: The stream power river incision model: Evidence, theory and beyond, Earth Surf. Process. Landforms, 39(1), 38–61, doi:10.1002/esp.3462, 2014.

Langston, A. L. and Temme, A. J. A. M.: Impacts of Lithologically Controlled Mechanisms on Downstream Bedrock Valley Widening, Geophys. Res. Lett., 46(21), 12056–12064, 2019.

Langston, A. L. and Tucker, G. E.: Developing and exploring a theory for the lateral erosion of bedrock channels for use in landscape evolution models, Earth Surf. Dyn., 6(1), 1–27, doi:10.5194/esurf-6-1-2018, 2018.

Lavé, J. and Avouac, J.-P.: Fluvial incision and tectonic uplift across the Himalayas of central Nepal, J. Geophys. Res. Solid Earth, 106(B11), 26561–26591, 2001.

Leopold, L. B. and Maddock, T. J.: The Hydraulic Geomtry of Stream Channels and Some Physiographic Implications, Geol. Surv. Prof. Pap. 252, 57, 1953.

Li, T., Fuller, T. K., Sklar, L. S., Gran, K. B. and Venditti, J. G.: A mechanistic model for lateral erosion of bedrock channel banks by bedload particle impacts, J. Geophys. Res. Earth Surf., 125(6), e2019JF005509, 2020.

Lóczy, D., Kis, É. and Schweitzer, F.: Local flood hazards assessed from channel morphometry along the Tisza River in Hungary, Geomorphology, 113(3), 200–209, doi:https://doi.org/10.1016/j.geomorph.2009.03.013, 2009.

Looper, J. P., Vieux, B. E. and Moreno, M. A.: Assessing the impacts of precipitation bias on distributed hydrologic model calibration and prediction accuracy, J. Hydrol., 418, 110–122, 2012.

Magilligan, F. J., Buraas, E. M. and Renshaw, C. E.: The efficacy of stream power and flow duration on geomorphic responses to catastrophic flooding, Geomorphology, 228, 175–188, 2015.

Manning, R., Griffith, J. P., Pigot, T. F. and Vernon-Harcourt, L. F.: On the flow of water in open channels and pipes., 1890.

Marcotte, A. L., Neudorf, C. M. and Langston, A. L.: Lateral bedrock erosion and valley formation in a heterogeneously layered landscape, Northeast Kansas, Earth Surf. Process. Landforms, 2021.

Mashael Al, S.: Assessment of flood hazard of Jeddah area 2009, Saudi Arabia, J. Water Resour. Prot., 2010, 2010.

May, C., Roering, J., Eaton, L. S. and Burnett, K. M.: Controls on valley width in mountainous landscapes : The role of landsliding and implications for salmonid habitat ABSTRACT, , 503–506, doi:10.1130/G33979.1, 2013.

Menier, D., Mathew, M., Pubellier, M., Sapin, F., Delcaillau, B., Siddiqui, N., Ramkumar, M. and Santosh, M.: Landscape response to progressive tectonic and climatic forcing in NW Borneo : Implications for geological and

geomorphic controls on flood hazard, , (December 2016), 1–18, doi:10.1038/s41598-017-00620-y, 2017.

Monegaglia, F., Zolezzi, G., Güneralp, I., Henshaw, A. J. and Tubino, M.: Environmental Modelling & Software Automated extraction of meandering river morphodynamics from multitemporal remotely sensed data, Environ. Model. Softw., 105, 171–186, doi:10.1016/j.envsoft.2018.03.028, 2018.

Montgomery, D. R.: Observations on the role of lithology in strath terrace formation and bedrock channel width, Am. J. Sci., 304(5), 454–476, doi:10.2475/ajs.304.5.454, 2004.

Montgomery, D. R. and Gran, K. B.: Downstream variations in the width of bedrock channels, Water Resour. Res., 37(6), 1841–1846, doi:10.1029/2000WR900393, 2001.

Morell, K. D., Styron, R., Stirling, M., Griffin, J., Archuleta, R. and Onur, T.: Seismic hazard analyses from geologic and geomorphic data: Current and future challenges, Tectonics, e2018TC005365, 2020.

O'Callaghan, J. F. and Mark, D. M.: The extraction of drainage networks from digital elevation data, Comput. Vision, Graph. Image Process., 27(2), 247, doi:10.1016/S0734-189X(84)80047-X, 1984.

Pechlivanidou, S., Cowie, P. A., Duclaux, G., Nixon, C. W., Gawthorpe, R. L. and Salles, T.: Tipping the balance: Shifts in sediment production in an active rift setting, Geology, 2019.

Plant, N. G., Flocks, J., Stockdon, H. F., Long, J. W., Guy, K., Thompson, D. M., Cormier, J. M., Smith, C. G. and Miselis, J. L.: Journal of Geophysical Research : Earth Surface, , 300–316, doi:10.1002/2013JF002871.Received, 2014.

Prince, P. S., Spotila, J. A. and Henika, W. S.: Stream capture as driver of transient landscape evolution in a tectonically quiescent setting, Geology, 39(9), 823–826, doi:10.1130/G32008.1, 2011.

Roux, C., Alber, A., Bertrand, M., Vaudor, L. and Piégay, H.: Geomorphology " FluvialCorridor " : A new ArcGIS toolbox package for multiscale riverscape exploration, Geomorphology, doi:10.1016/j.geomorph.2014.04.018, 2014.

Rowland, J. C., Shelef, E., Pope, P. A., Muss, J., Gangodagamage, C., Brumby, S. P. and Wilson, C. J.: Remote Sensing of Environment A morphology independent methodology for quantifying planview river change and characteristics from remotely sensed imagery, Remote Sens. Environ., 184, 212–228, doi:10.1016/j.rse.2016.07.005, 2016.

Sampson, C. C., Smith, A. M., Bates, P. D., Neal, J. C., Alfieri, L. and Freer, J. E.: A high-resolution global flood hazard model, Water Resour. Res., 51(9), 7358–7381, doi:doi:10.1002/2015WR016954, 2015.

Schanz, S. A. and Montgomery, D. R.: Geomorphology Lithologic controls on valley width and strath terrace formation, Geomorphology, 258, 58–68, doi:10.1016/j.geomorph.2016.01.015, 2016.

Schumm, S. A. and Ethridge, F. G.: Origin, evolution and morphology of fluvial valleys, 1994.

Sechu, G. L., Nilsson, B., Iversen, B. V, Greve, M. B., Børgesen, C. D. and Greve, M. H.: A stepwise gis approach for the delineation of river valley bottom within drainage basins using a cost distance accumulation analysis, Water (Switzerland), 13(6), doi:10.3390/w13060827, 2021.

Shelef, E. and Goren, L.: The rate and extent of wind-gap migration regulated by tributary confluences and avulsions, Earth Surf. Dyn., 687–700, 2021.

Shepherd, S. L., Dixon, J. C., Davis, R. K., Shepherd, S. L., Dixon, J. C., Davis, R. K., Ozark, A., Shepherd, S. L., Dixon, J. C. and Davis, R. K.: Are Ozark Streams Underfit ? Using Gis to Re- Examine Dury ' s Theory of Underfit

Streams RE-EXAMINE DURY ' S THEORY OF UNDERFIT STREAMS, , 3646(May), doi:10.2747/0272-3646.32.2.179, 2013.

Shobe, C. M., Tucker, G. E. and Barnhart, K. R.: The SPACE 1 . 0 model : a Landlab component for 2-D calculation of sediment transport , bedrock erosion , and landscape evolution, , 4577–4604, 2017.

Snyder, N. P. and Kammer, L. L.: Dynamic adjustments in channel width in response to a forced diversion : Gower Gulch , Death Valley National Park , California, , (2), 187–190, doi:10.1130/G24217A.1, 2008.

Snyder, N. P., Whipple, K. X., Tucker, G. E. and Merritts, D. J.: Channel response to tectonic forcing: Field analysis of stream morphology and hydrology in the Mendocino triple junction region, northern California, Geomorphology, 53(1–2), 97–127, doi:10.1016/S0169-555X(02)00349-5, 2003.

Spotila, J. A., Moskey, K. A. and Prince, P. S.: Geomorphology Geologic controls on bedrock channel width in large , slowly-eroding catchments : Case study of the New River in eastern North America, Geomorphology, 230, 51–63, doi:10.1016/j.geomorph.2014.11.004, 2015.

Sweeney, B. W., Bott, T. L., Jackson, J. K., Kaplan, L. A., Newbold, J. D., Standley, L. J., Hession, W. C. and Horwitz, R. J.: Riparian deforestation, stream narrowing, and loss of stream ecosystem services, Proc. Natl. Acad. Sci. U. S. A., 101(39), 14132 LP – 14137, doi:10.1073/pnas.0405895101, 2004.

Tomkin, J. H., Brandon, M. T., Pazzaglia, F. J., Barbour, J. R. and Willett, S. D.: Quantitative testing of bedrock incision models for the Clearwater River, NW Washington State, J. Geophys. Res. Solid Earth, 108(B6), doi:10.1029/2001jb000862, 2003.

Turowski, J. M.: Alluvial cover controlling the width, slope and sinuosity of bedrock channels, Earth Surf. Dyn., 6(1), 29–48, doi:10.5194/esurf-6-29-2018, 2018.

Turowski, J. M.: Mass balance, grade, and adjustment timescales in bedrock channels, Earth Surf. Dyn., 8(1), 103–122, doi:10.5194/esurf-8-103-2020, 2020.

Vaks, A., Woodhead, J., Bar-Matthews, M., Ayalon, A., Cliff, R. A., Zilberman, T., Matthews, A. and Frumkin, A.: Pliocene–Pleistocene climate of the northern margin of Saharan–Arabian Desert recorded in speleothems from the Negev Desert, Israel, Earth Planet. Sci. Lett., 368, 88–100, doi:https://doi.org/10.1016/j.epsl.2013.02.027, 2013.

Wessel, B.: TanDEM-X Ground Segment – DEM Products Specification Document, EOC, DLR, Oberpfaffenhofen, Germany, Public Document TD-GS-PS-0021, Issue 3.1. [online] Available from: https://tandemx-science.dlr.de/, 2016.

Whipple, K. X., Dibiase, R. A. and Crosby, B. T.: Chapter 254 - 9.28 Bedrock Rivers, Elsevier Ltd., 2013.

Whipple, K. X., Forte, A. M., DiBiase, R. A., Gasparini, N. M. and Ouimet, W. B.: Timescales of landscape response to divide migration and drainage capture: Implications for the role of divide mobility in landscape evolution, J. Geophys. Res. Earth Surf., 122(1), 248–273, 2017.

Whitbread, K., Jansen, J., Bishop, P. and Attal, M.: Substrate, sediment, and slope controls on bedrock channel geometry in postglacial streams, J. Geophys. Res. Earth Surf., 120(5), 779–798, doi:10.1002/2014JF003295, 2015.

Whittaker, A. C., Cowie, P. A., Attal, M., Tucker, G. E. and Roberts, G. P.: Bedrock channel adjustment to tectonic forcing: Implications for predicting river incision rates, Geology, 35(2), 103–106, doi:10.1130/G23106A.1, 2007a.

Whittaker, A. C., Cowie, P. A., Attal, M., Tucker, G. E. and Roberts, G. P.: Contrasting transient and steady-state

rivers crossing active normal faults: New field observations from the Central Apennines, Italy, Basin Res., 19(4), 529–556, 2007b.

Willett, S. D., McCoy, S. W., Perron, J. T., Goren, L. and Chen, C.-Y.: Dynamic reorganization of river basins, Science (80-.)., 343(6175), 1248765, 2014.

Wobus, C., Whipple, K. X., Kirby, E., Snyder, N., Johnson, J., Spyropolou, K., Crosby, B., Sheehan, D. and Willett, S. D.: Tectonics from topography: Procedures, promise, and pitfalls, Spec. Pap. Soc. Am., 398, 55, 2006.

Wohl, E. and Achyuthan, H.: Substrate influences on incised-channel morphology, J. Geol., 110(1), 115–120, 2002.

Wohl, E. and David, G. C. L.: Consistency of scaling relations among bedrock and alluvial channels, J. Geophys. Res. Earth Surf., 113(4), 1–16, doi:10.1029/2008JF000989, 2008.

Wright, M., Venditti, J. G., Li, T., Hurson, M., Chartrand, S., Rennie, C. and Church, M.: Covariation in width and depth in bedrock rivers, Earth Surf. Process. Landforms, (January), 1570–1582, doi:10.1002/esp.5335, 2022.

Yanites, B. J.: The Dynamics of Channel Slope, Width, and Sediment in Actively Eroding Bedrock River Systems, J. Geophys. Res. Earth Surf., 123(7), 1504–1527, doi:10.1029/2017JF004405, 2018.

Yanites, B. J., Tucker, G. E., Mueller, K. J., Chen, Y., Wilcox, T., Huang, S. and Shi, K.: Implications for the importance of channel width, , 3(7), 1192–1208, doi:10.1130/B30035.1, 2010.

Yanites, B. J., Ehlers, T. A., Becker, J. K., Schnellmann, M. and Heuberger, S.: High magnitude and rapid incision from river capture: Rhine River, Switzerland, J. Geophys. Res. Earth Surf., 118(2), 1060–1084, doi:10.1002/jgrf.20056, 2013.

Zilberman, E. and Calvo, R.: Journal of African Earth Sciences Remnants of Miocene fluvial sediments in the Negev Desert , Israel , and the Jordanian Plateau : Evidence for an extensive subsiding basin in the northwestern margins of the Arabian plate, J. African Earth Sci., 82, 33–53, doi:10.1016/j.jafrearsci.2013.02.006, 2013.

~~Allen, G. H., Barnes, J. B., Pavelsky, T. M. and Kirby, E.: Lithologic and tectonic controls on bedrock channel form at the northwest Himalayan front, J. Geophys. Res. Earth Surf., 118(3), 1806–1825, doi:10.1002/jgrf.20113, 2013.~~

~~Amit, R., Enzel, Y. and Sharon, D.: Permanent Quaternary hyperaridity in the Negev, Israel, resulting from regional tectonics blocking Mediterranean frontal systems, Geology, 34(6), 509–512 [online] Available from: http://dx.doi.org/10.1130/G22354.1, 2006.~~

~~Amit, R., Simhai, O., Ayalon, A., Enzel, Y., Matmon, A., Crouvi, O., Porat, N. and McDonald, E.: Transition from arid to hyper-arid environment in the southern Levant deserts as recorded by early Pleistocene cummulic Aridisols, Quat. Sci. Rev., 30(3), 312–323, doi:https://doi.org/10.1016/j.quascirev.2010.11.007, 2011.~~

~~Amos, C. B. and Burbank, D. W.: Channel width response to differential uplift, J. Geophys. Res. Earth Surf., 112(2), 1–11, doi:10.1029/2006JF000672, 2007.~~

~~Attal, M., Tucker, G. E., Whittaker, A. C., Cowie, P. A. and Roberts, G. P.: Modelling fluvial incision and transient landscape evolution: Influence of dynamic Channel adjustment, J. Geophys. Res. Earth Surf., 113(3), 1–16, doi:10.1029/2007JF000893, 2008.~~

~~Avni, Y., Bartov, Y., Garfunkel, Z. and Ginat, H.: Evolution of the Paran drainage basin and its relation to the Plio-~~

Pleistocene history of the Arava Rift western margin, Israel., Isr. J. Earth Sci., 49(4), 215–238, doi:10.1560/W8WL-JU3Y-KM7W-8LX4, 2000.

Avni, Y., Segev, A. and Ginat, H.: Oligocene regional denudation of the northern Afar dome: Pre- and syn-breakup stages of the Afro-Arabian plate, Bull. Geol. Soc. Am., 124(11–12), 1871–1897, doi:10.1130/B30634.1, 2012.

Beeson, H. W., Flitcroft, R. L., Fonstad, M. A. and Roering, J. J.: Deep-Seated Landslides Drive Variability in Valley Width and Increase Connectivity of Salmon Habitat in the Oregon Coast Range, JAWRA J. Am. Water Resour. Assoc., 54(6), 1325–1340, 2018.

Bertrand, M. and Liébault, F.: Active channel width as a proxy of sediment supply from mining sites in New Caledonia, Earth Surf. Process. Landforms, 44(1), 67–76, doi:https://doi.org/10.1002/esp.4478, 2019.

Bishop, P.: Drainage rearrangement by river capture, beheading and diversion, Prog. Phys. Geogr., 19(4), 449–473, doi:10.1177/030913339501900402, 1995.

Bitan, A. and Rubin, S.: Climatic atlas of Israel for physical and environmental planning and design, Minist. Transp. Jerusalem, 1991.

Brocard, G. Y. and van der Beek, P. A.: Influence of incision rate, rock strength, and bedload supply on bedrock river gradients and valley-flat widths: Field-based evidence and calibrations from western Alpine rivers (southeast France), S. D. Willett al., Spec. Pap. Geol. Soc. Am, 398, 101–126, 2006.

Brussock, P. P., Brown, A. V and Dixon, J. C.: CHANNEL FORM AND STREAM ECOSYSTEM MODELS, JAWRA J. Am. Water Resour. Assoc., 21(5), 859–866, doi:10.1111/j.1752-1688.1985.tb00180.x, 1985.

Clubb, F. J., Mudd, S. M., Milodowski, D. T., Valters, D. A., Slater, L. J., Hurst, M. D. and Limaye, A. B.: Geomorphometric delineation of floodplains and terraces from objectively defined topographic thresholds, Earth Surf. Dyn., 5(3), 369–385, doi:10.5194/esurf-5-369-2017, 2017.

Clubb, F. J., Weir, E. F. and Mudd, S. M.: Continuous measurements of valley floor width in mountainous landscapes, , (February), 1–27, 2022.

Davis, W. M.: A river-pirate, Science (80-.)., 13, 108–109, 1889.

DiBiase, R. A. and Whipple, K. X.: The influence of erosion thresholds and runoff variability on the relationships among topography, climate, and erosion rate, J. Geophys. Res. Earth Surf., 116(F4), doi:https://doi.org/10.1029/2011JF002095, 2011.

Dunne, T. and Leopold, L. B.: Water in environmental planning, Macmillan., 1978.

Dury, G. H.: Principles of underfit streams, US Government Printing Office., 1964.

Fan, N., Chu, Z., Jiang, L., Hassan, M. A., Lamb, M. P. and Liu, X.: Abrupt drainage basin reorganization following a Pleistocene river capture, Nat. Commun., 9(1), 1–6, 2018.

Faustini, J. M., Kaufmann, P. R. and Herlihy, A. T.: Downstream variation in bankfull width of wadeable streams across the conterminous United States, Geomorphology, 108(3–4), 292–311, doi:10.1016/J.GEOMORPH.2009.02.005, 2009.

Finnegan, N. J. and Balco, G.: Sediment supply, base level, braiding, and bedrock river terrace formation: Arroyo Seco, California, USA, Bull. Geol. Soc. Am., 125(7–8), 1114–1124, doi:10.1130/B30727.1, 2013.

Finnegan, N. J., Roe, G., Montgomery, D. R. and Hallet, B.: Controls on the channel width of rivers: Implications for

modeling fluvial incision of bedrock, Geology, 33(3), 229–232, doi:10.1130/G21171.1, 2005.

Fisher, G. B., Bookhagen, B. and Amos, C. B.: Channel planform geometry and slopes from freely available high-spatial resolution imagery and DEM fusion: Implications for channel width scalings, erosion proxies, and fluvial signatures in tectonically active landscapes, Geomorphology, 194, 46–56, doi:10.1016/j.geomorph.2013.04.011, 2013.

Flint, J. J.: Stream gradient as a function of order, magnitude, and discharge, Water Resour. Res., 10(5), 969–973, doi:10.1029/WR010i005p00969, 1974.

Fryirs, K. A., Brierley, G. J., Wheaton, J. M., Bizzi, S. and Williams, R.: To plug-in or not to plug-in ? Geomorphic analysis of rivers using the River Styles Framework in an era of big data acquisition and automation, , (June), 1–20, doi:10.1002/wat2.1372, 2019.

Garfunkel, Z.: Internal structure of the Dead Sea leaky transform (rift) in relation to plate kinematics, Tectonophysics, 80(1–4), 81–108, 1981.

Garfunkel, Z. and Horowitz, A.: The upper Tertiary and Quaternary morphology of the Negev, Israel, Isr. J. Earth Sci, 15(3), 101–117, 1966.

Garfunkel, Z., Ben-Avraham, Z. and Kagen, E.: Dead Sea Transform Fault System : Reviews., 2014.

Giaconia, F., Booth-Rea, G., Martínez-Martínez, J. M., Azañón, J. M., Pérez-Peña, J. V., Pérez-Romero, J. and Villegas, I.: Geomorphic evidence of active tectonics in the Sierra Alhamilla (eastern Betics, SE Spain), Geomorphology, 145–146, 90–106, doi:https://doi.org/10.1016/j.geomorph.2011.12.043, 2012.

Gibling, M. R.: Width and Thickness of Fluvial Channel Bodies and Valley Fills in the Geological Record: A Literature Compilation and Classification, J. Sediment. Res., 76(5), 731–770, doi:10.2110/jsr.2006.060, 2006.

Gilbert, J. T., Macfarlane, W. W. and Wheaton, J. M.: The Valley Bottom Extraction Tool (V-BET): A GIS tool for delineating valley bottoms across entire drainage networks, Comput. Geosci., 97, 1–14, doi:10.1016/j.cageo.2016.07.014, 2016.

Ginat, H.: The geology and geomorphology of Yotvata Region, Isr. Geol. Surv. Rep. GSI/8/91, 1991.

Ginat, H., Zilberman, E. and Avni, Y.: Tectonic and paleogeographic significance of the Edom River , a Pliocene stream that crossed the Dead Sea Rift valley, Isr. J. Earth Sci., 49(1), 159–177, doi:10.1560/N2P9-YBJ0-Q44Y-GWYN, 2000.

Ginat, H., Zilberman, E. and Amit, R.: Red sedimentary units as indicators of Early Pleistocene tectonic activity in the southern Negev desert, Israel, Geomorphology, 45(1–2), 127–146, doi:10.1016/S0169-555X(01)00193-3, 2002.

Ginat, H., Opitz, S., Ababneh, L., Faershtein, G., Lazar, M., Porat, N. and Mischke, S.: Pliocene-Pleistocene waterbodies and associated deposits in southern Israel and southern Jordan, J. Arid Environ., 148, 14–33, doi:10.1016/j.jaridenv.2017.09.007, 2018.

Golly, A. and Turowski, J. M.: Deriving principal channel metrics from bank and long-profile geometry with the R package cmgo, Earth Surf. Dyn., 5(3), 557–570, 2017.

Goren, L., Willett, S. D., Herman, F. and Braun, J.: Coupled numerical-analytical approach to landscape evolution modeling, Earth Surf. Process. Landforms, 39(4), 522–545, doi:10.1002/esp.3514, 2014.

Guralnik, B., Matmon, A., Avni, Y. and Fink, D.: 10Be exposure ages of ancient desert pavements reveal Quaternary

evolution of the Dead Sea drainage basin and rift margin tilting, Earth Planet. Sci. Lett., 290(1–2), 132–141, doi:10.1016/j.epsl.2009.12.012, 2010.

Hancock, G. S. and Anderson, R. S.: Numerical modeling of fluvial strath-terrace formation in response to oscillating climate, , (9), 1131–1142, 2002.

Harbor, D. J.: Dynamic equilibrium between an active uplift and the Sevier River, Utah, J. Geol., 106(2), 181–194, 1998.

Harel, E., Goren, L., Shelef, E. and Ginat, H.: Drainage reversal toward cliffs induced by lateral lithologic differences, Geology, 2019.

Haviv, I., Enzel, Y., Whipple, K. X., Zilberman, E., Matmon, A., Stone, J. and Fifield, K. L.: Evolution of vertical knickpoints (waterfalls) with resistant caprock: Insights from numerical modeling, J. Geophys. Res. Earth Surf., 115(F3), doi:https://doi.org/10.1029/2008JF001187, 2010.

Hilley, G. E., Baden, C. W., Dobbs, S. C., Plante, Z., Sare, R. and Steelquist, A. T.: A Curvature-Based Method for Measuring Valley Width Applied to Glacial and Fluvial Landscapes, J. Geophys. Res. Earth Surf., 125(12), e2020JF005605, doi:https://doi.org/10.1029/2020JF005605, 2020.

Jones, J. C.: Historical channel change caused by a century of flow alteration on Sixth Water Creek and Diamond Fork River, UT, Utah State University., 2018.

Keen-Zebert, A., Hudson, M. R., Shepherd, S. L. and Thaler, E. A.: The effect of lithology on valley width, terrace distribution, and bedload provenance in a tectonically stable catchment with flat-lying stratigraphy, Earth Surf. Process. Landforms, 42(10), 1573–1587, doi:10.1002/esp.4116, 2017.

Kirby, E. and Ouimet, W.: Tectonic geomorphology along the eastern margin of Tibet: Insights into the pattern and processes of active deformation adjacent to the Sichuan Basin, Geol. Soc. Spec. Publ., 353, 165–188, doi:10.1144/SP353.9, 2011.

Lague, D.: The stream power river incision model: Evidence, theory and beyond, Earth Surf. Process. Landforms, 39(1), 38–61, doi:10.1002/esp.3462, 2014.

Langston, A. L. and Temme, A. J. A. M.: Impacts of Lithologically Controlled Mechanisms on Downstream Bedrock Valley Widening, Geophys. Res. Lett., 46(21), 12056–12064, 2019.

Langston, A. L. and Tucker, G. E.: Developing and exploring a theory for the lateral erosion of bedrock channels for use in landscape evolution models, Earth Surf. Dyn., 6(1), 1–27, doi:10.5194/esurf-6-1-2018, 2018.

Lavé, J. and Avouac, J. P.: Fluvial incision and tectonic uplift across the Himalayas of central Nepal, J. Geophys. Res. Solid Earth, 106(B11), 26561–26591, 2001.

Leopold, L. B. and Maddock, T. J.: The Hydraulic Geomtry of Stream Channels and Some Physiographic Implications, Geol. Surv. Prof. Pap. 252, 57, 1953.

Li, T., Fuller, T. K., Sklar, L. S., Gran, K. B. and Venditti, J. G.: A mechanistic model for lateral erosion of bedrock channel banks by bedload particle impacts, J. Geophys. Res. Earth Surf., 125(6), e2019JF005509, 2020.

Lóczy, D., Kis, É. and Schweitzer, F.: Local flood hazards assessed from channel morphometry along the Tisza River in Hungary, Geomorphology, 113(3), 200–209, doi:https://doi.org/10.1016/j.geomorph.2009.03.013, 2009.

Looper, J. P., Vieux, B. E. and Moreno, M. A.: Assessing the impacts of precipitation bias on distributed hydrologic

model calibration and prediction accuracy, J. Hydrol., 418, 110–122, 2012.

Magilligan, F. J., Buraas, E. M. and Renshaw, C. E.: The efficacy of stream power and flow duration on geomorphic responses to catastrophic flooding, Geomorphology, 228, 175–188, 2015.

Manning, R., Griffith, J. P., Pigot, T. F. and Vernon-Harcourt, L. F.: On the flow of water in open channels and pipes., 1890.

Marcotte, A. L., Neudorf, C. M. and Langston, A. L.: Lateral bedrock erosion and valley formation in a heterogeneously layered landscape, Northeast Kansas, Earth Surf. Process. Landforms, 2021.

Mashael Al, S.: Assessment of flood hazard of Jeddah area 2009, Saudi Arabia, J. Water Resour. Prot., 2010, 2010.

May, C., Roering, J., Eaton, L. S. and Burnett, K. M.: Controls on valley width in mountainous landscapes : The role of landsliding and implications for salmonid habitat ABSTRACT, , 503–506, doi:10.1130/G33979.1, 2013.

Menier, D., Mathew, M., Pubellier, M., Sapin, F., Delcaillau, B., Siddiqui, N., Ramkumar, M. and Santosh, M.: Landscape response to progressive tectonic and climatic forcing in NW Borneo : Implications for geological and geomorphic controls on flood hazard, , (December 2016), 1–18, doi:10.1038/s41598-017-00620-y, 2017.

Monegaglia, F., Zolezzi, G., Güneralp, I., Henshaw, A. J. and Tubino, M.: Environmental Modelling & Software Automated extraction of meandering river morphodynamics from multitemporal remotely sensed data, Environ. Model. Softw., 105, 171–186, doi:10.1016/j.envsoft.2018.03.028, 2018.

Montgomery, D. R.: Observations on the role of lithology in strath terrace formation and bedrock channel width, Am. J. Sci., 304(5), 454–476, doi:10.2475/ajs.304.5.454, 2004.

Montgomery, D. R. and Gran, K. B.: Downstream variations in the width of bedrock channels, Water Resour. Res., 37(6), 1841–1846, doi:10.1029/2000WR900393, 2001.

Morell, K. D., Styron, R., Stirling, M., Griffin, J., Archuleta, R. and Onur, T.: Seismic hazard analyses from geologic and geomorphic data: Current and future challenges, Tectonics, e2018TC005365, 2020.

O'Callaghan, J. F. and Mark, D. M.: The extraction of drainage networks from digital elevation data, Comput. Vision, Graph. Image Process., 27(2), 247, doi:10.1016/S0734-189X(84)80047-X, 1984.

Pechlivanidou, S., Cowie, P. A., Duclaux, G., Nixon, C. W., Gawthorpe, R. L. and Salles, T.: Tipping the balance: Shifts in sediment production in an active rift setting, Geology, 2019.

Phillips, J. D.: Drainage area and incised valley fills in Texas rivers: A potential explanation, Sediment. Geol., 242(1), 65–70, doi:https://doi.org/10.1016/j.sedgeo.2011.10.007, 2011.

Plant, N. G., Flocks, J., Stockdon, H. F., Long, J. W., Guy, K., Thompson, D. M., Cormier, J. M., Smith, C. G. and Miselis, J. L.: Journal of Geophysical Research : Earth Surface, , 300–316, doi:10.1002/2013JF002871.Received, 2014.

Prince, P. S., Spotila, J. A. and Henika, W. S.: Stream capture as driver of transient landscape evolution in a tectonically quiescent setting, Geology, 39(9), 823–826, doi:10.1130/G32008.1, 2011.

Roux, C., Alber, A., Bertrand, M., Vaudor, L. and Piégay, H.: Geomorphology " FluvialCorridor " : A new ArcGIS toolbox package for multiscale riverscape exploration, Geomorphology, doi:10.1016/j.geomorph.2014.04.018, 2014.

Rowland, J. C., Shelef, E., Pope, P. A., Muss, J., Gangodagamage, C., Brumby, S. P. and Wilson, C. J.: Remote Sensing of Environment A morphology independent methodology for quantifying planview river change and

characteristics from remotely sensed imagery, Remote Sens. Environ., 184, 212–228, doi:10.1016/j.rse.2016.07.005, 2016.

Sampson, C. C., Smith, A. M., Bates, P. D., Neal, J. C., Alfieri, L. and Freer, J. E.: A high-resolution global flood hazard model, Water Resour. Res., 51(9), 7358–7381, doi:doi:10.1002/2015WR016954, 2015.

Schanz, S. A. and Montgomery, D. R.: Geomorphology Lithologic controls on valley width and strath terrace formation, Geomorphology, 258, 58–68, doi:10.1016/j.geomorph.2016.01.015, 2016.

Schumm, S. A. and Ethridge, F. G.: Origin, evolution and morphology of fluvial valleys, 1994.

Sechu, G. L., Nilsson, B., Iversen, B. V, Greve, M. B., Børgesen, C. D. and Greve, M. H.: A stepwise gis approach for the delineation of river valley bottom within drainage basins using a cost distance accumulation analysis, Water (Switzerland), 13(6), doi:10.3390/w13060827, 2021.

Shelef, E. and Goren, L.: The rate and extent of wind gap migration regulated by tributary confluences and avulsions, Earth Surf. Dyn., 687–700, 2021.

Shobe, C. M., Tucker, G. E. and Barnhart, K. R.: The SPACE 1 . 0 model : a Landlab component for 2 D calculation of sediment transport , bedrock erosion , and landscape evolution, , 4577–4604, 2017.

Snyder, N. P. and Kammer, L. L.: Dynamic adjustments in channel width in response to a forced diversion : Gower Gulch , Death Valley National Park , California, , (2), 187–190, doi:10.1130/G24217A.1, 2008.

Snyder, N. P., Whipple, K. X., Tucker, G. E. and Merritts, D. J.: Channel response to tectonic forcing: Field analysis of stream morphology and hydrology in the Mendocino triple junction region, northern California, Geomorphology, 53(1–2), 97–127, doi:10.1016/S0169-555X(02)00349-5, 2003.

Spotila, J. A., Moskey, K. A. and Prince, P. S.: Geomorphology Geologic controls on bedrock channel width in large , slowly eroding catchments : Case study of the New River in eastern North America, Geomorphology, 230, 51–63, doi:10.1016/j.geomorph.2014.11.004, 2015.

Sweeney, B. W., Bott, T. L., Jackson, J. K., Kaplan, L. A., Newbold, J. D., Standley, L. J., Hession, W. C. and Horwitz, R. J.: Riparian deforestation, stream narrowing, and loss of stream ecosystem services, Proc. Natl. Acad. Sci. U. S. A., 101(39), 14132 LP – 14137, doi:10.1073/pnas.0405895101, 2004.

Tomkin, J. H., Brandon, M. T., Pazzaglia, F. J., Barbour, J. R. and Willett, S. D.: Quantitative testing of bedrock incision models for the Clearwater River, NW Washington State, J. Geophys. Res. Solid Earth, 108(B6), doi:10.1029/2001jb000862, 2003.

Turowski, J. M.: Alluvial cover controlling the width, slope and sinuosity of bedrock channels, Earth Surf. Dyn., 6(1), 29–48, doi:10.5194/esurf-6-29-2018, 2018.

Turowski, J. M.: Mass balance, grade, and adjustment timescales in bedrock channels, Earth Surf. Dyn., 8(1), 103–122, doi:10.5194/esurf-8-103-2020, 2020.

Vaks, A., Woodhead, J., Bar-Matthews, M., Ayalon, A., Cliff, R. A., Zilberman, T., Matthews, A. and Frumkin, A.: Pliocene–Pleistocene climate of the northern margin of Saharan–Arabian Desert recorded in speleothems from the Negev Desert, Israel, Earth Planet. Sci. Lett., 368, 88–100, doi:https://doi.org/10.1016/j.epsl.2013.02.027, 2013.

Wessel, B.: TanDEM-X Ground Segment – DEM Products Specification Document, EOC, DLR, Oberpfaffenhofen, Germany, Public Document TD-GS-PS-0021, Issue 3.1. [online] Available from: https://tandemx-science.dlr.de/,

2016.

Whipple, K. X., Dibiase, R. A. and Crosby, B. T.: Chapter 254 – 9.28 Bedrock Rivers, Elsevier Ltd., 2013.

Whitbread, K., Jansen, J., Bishop, P. and Attal, M.: Substrate, sediment, and slope controls on bedrock channel geometry in postglacial streams, J. Geophys. Res. Earth Surf., 120(5), 779–798, doi:10.1002/2014JF003295, 2015.

Whittaker, A. C., Cowie, P. A., Attal, M., Tucker, G. E. and Roberts, G. P.: Bedrock channel adjustment to tectonic forcing: Implications for predicting river incision rates, Geology, 35(2), 103–106, doi:10.1130/G23106A.1, 2007a.

Whittaker, A. C., Cowie, P. A., Attal, M., Tucker, G. E. and Roberts, G. P.: Contrasting transient and steady-state rivers crossing active normal faults: New field observations from the Central Apennines, Italy, Basin Res., 19(4), 529–556, 2007b.

Willett, S. D., McCoy, S. W., Perron, J. T., Goren, L. and Chen, C. Y.: Dynamic reorganization of river basins, Science (80-.)., 343(6175), 1248765, 2014.

Wobus, C., Whipple, K. X., Kirby, E., Snyder, N., Johnson, J., Spyropolou, K., Crosby, B., Sheehan, D. and Willett, S. D.: Tectonics from topography: Procedures, promise, and pitfalls, Spec. Pap. Soc. Am., 398, 55, 2006.

Wohl, E. and Achyuthan, H.: Substrate influences on incised-channel morphology, J. Geol., 110(1), 115–120, 2002.

Wohl, E. and David, G. C. L.: Consistency of scaling relations among bedrock and alluvial channels, J. Geophys. Res. Earth Surf., 113(4), 1–16, doi:10.1029/2008JF000989, 2008.

Wright, M., Venditti, J. G., Li, T., Hurson, M., Chartrand, S., Rennie, C. and Church, M.: Covariation in width and depth in bedrock rivers, Earth Surf. Process. Landforms, (January), 1570–1582, doi:10.1002/esp.5335, 2022.

Yanites, B. J.: The Dynamics of Channel Slope, Width, and Sediment in Actively Eroding Bedrock River Systems, J. Geophys. Res. Earth Surf., 123(7), 1504–1527, doi:10.1029/2017JF004405, 2018.

Yanites, B. J., Tucker, G. E., Mueller, K. J., Chen, Y., Wilcox, T., Huang, S. and Shi, K.: Implications for the importance of channel width, , 3(7), 1192–1208, doi:10.1130/B30035.1, 2010.

Yanites, B. J., Ehlers, T. A., Becker, J. K., Schnellmann, M. and Heuberger, S.: High magnitude and rapid incision from river capture: Rhine River, Switzerland, J. Geophys. Res. Earth Surf., 118(2), 1060–1084, doi:10.1002/jgrf.20056, 2013.

Zilberman, E. and Calvo, R.: Journal of African Earth Sciences Remnants of Miocene fluvial sediments in the Negev Desert , Israel , and the Jordanian Plateau : Evidence for an extensive subsiding basin in the northwestern margins of the Arabian plate, J. African Earth Sci., 82, 33–53, doi:10.1016/j.jafrearsci.2013.02.006, 2013.